ANL/NDM--87

DE85 000293

ANL/NDM-87
CROSS-SECTION MEASUREMENT FOR THE $^{7}Li(n,n't)^{4}He$ REACTION AT 14.74 MeV*

by

Donald L. Smith, James W. Meadows, Manuel M. Bretscher and Samson A. Cox

September 1984

E NUCLEAR REACTION $^{7}Li(n,n't)^{4}He$. Measured $\sigma_{nn't}$ relative to the ^{238}U neutron-fission cross section at 14.74 MeV. Determined tritium activity by a liquid-scintillation counting method. Detailed uncertainty analysis. Compared result with data and recent evaluations from the literature.

Applied Physics Division
Argonne National Laboratory
9700 South Cass Avenue
Argonne, Illinois 60439
USA

* This work supported by the U.S. Department of Energy.

NUCLEAR DATA AND MEASUREMENTS SERIES

The Nuclear Data and Measurements Series presents results of studies in the field of microscopic nuclear data. The primary objective is the dissemination of information in the comprehensive form required for nuclear technology applications. This Series is devoted to: a) measured microscopic nuclear parameters, b) experimental techniques and facilities employed in measurements, c) the analysis, correlation and interpretation of nuclear data, and d) the evaluation of nuclear data. Contributions to this Series are reviewed to assure technical competence and, unless otherwise stated, the contents can be formally referenced. This Series does not supplant formal journal publication but it does provide the more extensive information required for technological applications (e.g., tabulated numerical data) in a timely manner.

INFORMATION ABOUT OTHER ISSUES IN THE ANL/NDM SERIES:

A list of titles and authors for reports ANL/NDM-1 through ANL/NDM-50 can be obtained by referring to any report of this series numbered ANL/NDM-51 through ANL/NDM-76. Requests for a complete list of titles or for copies of previous reports should be directed to:

Section Secretary
Applied Nuclear Physics Section
Applied Physics Division
Building 316
Argonne National Laboratory
9700 South Cass Avenue
Argonne, Illinois 60439
USA

ANL/NDM-51 Measured and Evaluated Neutron Cross Sections of Elemental Bismuth by A. Smith, P. Guenther, D. Smith and J. Whalen, April 1980.

ANL/NDM-52 Neutron Total and Scattering Cross Sections of ^{6}Li in the Few MeV Region by P. Guenther, A. Smith and J. Whalen, February 1980.

ANL/NDM-53 Neutron Source Investigations in Support of the Cross Section Program at the Argonne Fast-Neutron Generator by James W. Meadows and Donald L. Smith, May 1980.

ANL/NDM-54 The Nonelastic-Scattering Cross Sections of Elemental Nickel by A. B. Smith, P. T. Guenther and J. F. Whalen, June 1980.

ANL/NDM-55 Thermal Neutron Calibration of a Tritium Extraction Facility using the $^{6}Li(n,t)^{4}He/^{197}Au(n,\gamma)^{198}Au$ Cross Section Ratio for Standardization by M. M. Bretscher and D. L. Smith, August 1980.

ANL/NDM-56 Fast-Neutron Interactions with ^{182}W, ^{184}W and ^{186}W by P. T. Guenther, A. B. Smith and J. F. Whalen, December 1980.

ANL/NDM-57 The Total, Elastic- and Inelastic-Scattering Fast-Neutron Cross Sections of Natural Chromium by Peter T. Guenther, Alan B. Smith and James F. Whalen, January 1981.

ANL/NDM-58 Review of Measurement Techniques for the Neutron Capture Process by W. P. Poenitz, August 1981.

ANL/NDM-59 Review of the Importance of the Neutron Capture Process in Fission Reactors by Wolfgang P. Poenitz, July 1981.

ANL/NDM-60 Gamma-Ray Detector Calibration Methods Utilized in the Argonne FNG Group Activation Cross Section Measurement Program by James W. Meadows and Donald L. Smith, April 1984.

ANL/NDM-61 Fast-neutron Total and Scattering Cross Sections of ^{58}Ni by Carl Budtz-Jørgensen, Peter T. Guenther, Alan B. Smith and James F. Whalen, September 1981.

ANL/NDM-62 Covariance Matrices and Applications to the Field of Nuclear Data by Donald L. Smith, November 1981.

ANL/NDM-63 On Neutron Inelastic-Scattering Cross Sections of ^{232}Th, ^{233}U, ^{235}U, ^{238}U, ^{239}U, and ^{239}Pu and ^{240}Pu by Alan B. Smith and Peter T. Guenther, January 1982.

ANL/NDM-64 The Fission-Fragment Angular Distributions and Total Kinetic Energies for ^{235}U(n,f) from 0.18 to 8.83 MeV by James W. Meadows and Carl Budtz-Jørgensen, January 1982.

ANL/NDM-65 Note on the Elastic Scattering of Several-MeV Neutrons from Elemental Calcium by Alan B. Smith and Peter T. Guenther, March 1982.

ANL/NDM-66 Fast-neutron Scattering Cross Sections of Elemental Silver by Alan B. Smith and Peter T. Guenther, May 1982.

ANL/NDM-67 Non-evaluation Applications for Covariance Matrices by Donald L. Smith, July 1982.

ANL/NDM-68 Fast-neutron Total and Scattering Cross Sections of ^{103}Rh by Alan B. Smith, Peter T. Guenther and James F. Whalen, July 1982.

ANL/NDM-69 Fast-neutron Scattering Cross Sections of Elemental Zirconium by Alan B. Smith and Peter T. Guenther, December 1982.

ANL/NDM-70 Fast-neutron Total and Scattering Cross Sections of Niobium by Alan B. Smith, Peter T. Guenther and James F. Whalen, July 1982.

ANL/NDM-71 Fast-neutron Total and Scattering Cross Sections of Elemental Palladium by Alan B. Smith, Peter T. Guenther and James F. Whalen, June 1982.

ANL/NDM-72 Fast-neutron Scattering from Elemental Cadmium by Alan B. Smith and Peter T. Guenther, July 1982.

ANL/NDM-73 Fast-neutron Elastic-Scattering Cross Sections of Elemental Tin by C. Budtz-Jørgensen, Peter T. Guenther and Alan B. Smith, July 1982.

ANL/NDM-74 Evaluation of the ^{238}U Neutron Total Cross Section by Wolfgang Poenitz, Alan B. Smith and Robert Howerton, December 1982.

ANL/NDM-75 Neutron Total and Scattering Cross Sections of Elemental Antimony by Alan B. Smith, Peter T. Guenther and James F. Whalen, September 1982.

ANL/NDM-76 Scattering of Fast-Neutrons from Elemental Molybdenum by Alan B. Smith and Peter T. Guenther, November 1982.

ANL/NDM-77 A Least-Squares Method for Deriving Reaction Differential Cross Section Information from Measurements Performed in Diverse Neutron Fields by Donald L. Smith, November 1982.

ANL/NDM-78 Fast-Neutron Total and Elastic-Scattering Cross Sections of Elemental Indium by A. B. Smith, P. T. Guenther, and J. F. Whalen, November 1982.

ANL/NDM-79 Few-MeV Neutrons Incident on Yttrium by C. Budtz-Jørgensen, P. Guenther, A. Smith and J. Whalen, June 1983.

ANL/NDM-80 Neutron Total Cross Section Measurements in the Energy Region from 47 keV to 20 MeV by W. P. Poenitz and J. F. Whalen, July 1983.

ANL/NDM-81 Covariances for Neutron Cross Sections Calculated Using a Regional Model Based on Elemental-Model Fits to Experimental Data by Donald L. Smith and Peter T. Guenther, November 1983.

ANL/NDM-82 Reaction Differential Cross Sections from the Least-Squares Unfolding of Ratio Data Measured in Diverse Neutron Fields by Donald L. Smith, January 1984.

ANL/NDM-83 The Fission Cross Sections of Some Thorium, Uranium, Neptunium and Plutonium Isotopes Relative to ^{235}U by J. W. Meadows, October 1983.

ANL/NDM-84 ^{235}U and ^{239}Pu Sample-Mass Determinations and Intercomparisons by W. P. Poenitz and J. W. Meadows, November 1983.

ANL/NDM-85 Measurement of the $^{51}V(n,p)^{51}Ti$ Reaction Cross Section from Threshold to 9.3 MeV by the Activation Method by Donald L. Smith, James W. Meadows and Ikuo Kanno, June 1984.

ANL/NDM-86 Energy-Differential Cross Section Measurement for the $^{51}V(n,\alpha)^{48}Sc$ Reaction by Ikuo Kanno, James W. Meadows and Donald L. Smith, August 1984.

TABLE OF CONTENTS

CROSS-SECTION MEASUREMENT FOR THE $^{7}Li(n,n't)^{4}He$ REACTION AT 14.74 MeV*

by

Donald L. Smith, James W. Meadows,
Manuel M. Bretscher and Samson A. Cox

Applied Physics Division
Argonne National Laboratory
9700 South Cass Avenue
Argonne, Illinois 60439
U.S.A.

ABSTRACT

The cross section for the $^{7}Li(n,n't)^{4}He$ reaction is measured at an average neutron energy of 14.74 MeV, with a resolution of 0.324 MeV, relative to the ^{238}U neutron-fission cross section. Tritium activities for the irradiated lithium-metal samples (enriched to 99.95% in ^{7}Li) are deduced using a liquid-scintillation counting method which relies upon the tritiated-water standard from the U.S. National Bureau of Standards. The measured cross section ratio of $^{7}Li(n,n't)^{4}He$ to ^{238}U neutron fission is 0.2523 (± 2.2%). The derived $^{7}Li(n,n't)^{4}He$ reaction cross section is 0.301 (± 5.3%) barn, based on the ENDF/B-V value of 1.193 (± 4.8%) barn for the ^{238}U neutron-fission cross section.

*This work supported by the U. S. Department of Energy

I. INTRODUCTION

An important technical and economic issue for fusion reactors designed to employ the DT fuel cycle is the availability of tritium fuel. Since tritium has a half life of only ~ 12 years, it is not found naturally in significant amounts and must be produced. The breeding of tritium via the $^{6}Li(n,t)^{4}He$ and $^{7}Li(n,n't)^{4}He$ reactions in a lithium-bearing blanket surrounding the reactor is the method envisioned for current conceptual designs [1]. It is imperative that the tritium breeding ratio (TBR) exceed unity, i.e., that DT fusion reactors produce more tritium than they consume. In the 1960's, conceptual designs involving natural lithium blankets were predicting TBR ~ 1.3 to 1.5 so there was little concern regarding this matter. However, considerations of safety eventually led designers to reject pure lithium blanket concepts and instead to propose solid lithium compounds. Natural lithium is very reactive, and the potential risk of tritium release from blanket fires is a matter to be avoided. For compounds, the design calculations lead to TBR relatively close to unity. Thus by the late 1970's accurate knowledge of the cross sections for neutron-induced production of tritium in lithium became an essential engineering requirement. This need persists and it is reflected in formal requests for nuclear data (e.g., Refs. 2 and 3).

The relative importance of the $^{6}Li(n,t)^{4}He$ and $^{7}Li(n,n't)^{4}He$ reactions depends strongly on blanket design [1]. Some designs involve mainly light-element compounds (e.g., O, Al, Si), with Be used as a neutron multiplier to help increase the TBR. For these designs, the exoergic reaction $^{6}Li(n,t)^{4}He$ is the predominent source of tritium, in spite of the low abundance of ^{6}Li, due to the large response of this reaction to the relatively-low average neutron energy characteristic of the associated spectra. Other proposed reactor designs involve significant heavy-element content in the blankets. In particular, Pb and Bi compounds are favored as neutron multipliers. The neutron spectra in these designs are considerably harder so the endoergic $^{7}Li(n,n't)^{4}He$ reaction plays a significant role.

The $^{6}Li(n,t)^{4}He$ reaction has been used for many years as a standard for neutron cross section measurements (e.g., Ref. 4). In this context it has been widely investigated, and it is generally agreed that the cross section is adequately known for fusion-energy applications [1]. Thus, attention has been focused lately on the $^{7}Li(n,n't)^{4}He$ reaction. The status prior to 1979 was reviewed by both Swinhoe [5] and Haight [6]. ENDF/B-IV [7] appeared to adequately represent the available data at that time; however, the experimental values generally carried large errors and, for the most part, tended to scatter in excess of the reported errors. Swinhoe and Uttley [5,8] recognized the importance of this cross section, and its contemporary relative uncertainty, and carried out a comprehensive set of measurements using tritium-detection techniques. On the basis of their work, they alerted the nuclear data community to the fact that the then-accepted cross section values were probably too large. Their results were a source of considerable concern to the nuclear data community since cross sections systematically lower than

ENDF/B-IV [7] by ~ 25% were found over the energy range 5-14 MeV. This implied sharply reduced TBR values, possibly less than unity for some designs [5]. The surprising results of Refs. 5 and 8 stimulated measurements at Argonne National Laboratory and elsewhere. The first work to be published was that from Argonne by Smith et al. [9,10]. Seven data points in the energy range ~ 7-9 MeV were reported. In this energy range the $^{7}Li(n,n't)^{4}He$ cross section appears to reach a maximum and shows little energy dependence. An average of 0.372 (± 3.8%) barn was reported for this set, based on errors of ~ 5-6% for the individual measured values. These cross sections fall nearly midway between the values of Swinhoe and Uttley [5,8] and ENDF/B-IV [7]. The results of an experiment at CBNM by Liskien and Paulsen [11] were published shortly after the Argonne work. A direct-detection technique was employed, with values spanning the range 6-10 MeV. The uncertainties associated with this technique are larger than for activation measurements, and the errors quoted are in the range 11-19%. The data of Liskien and Paulsen [11] are consistent with the work of Smith et al. [9,10], and are systematically lower than ENDF/B-IV [7] and higher than the values of Swinhoe and Uttley [5,8]. The average of the three data points of Liskien and Paulsen [11] which cover the 7-9 MeV energy range (each has ~ 12% error) is 0.368 barn, in excellent agreement with the corresponding average reported by Smith et al. [9,10]. In 1979 ENDF/B-V [12] was released. For the $^{7}Li(n,n't)^{4}He$ reaction this version was a direct carry over from ENDF/B-IV, since the above-mentioned new results were not available. In 1981 another ^{7}Li evaluation was prepared by Young [13]. This evaluation employed an unbiased least-squares method which simultaneously considered the total, elastic scattering, inelastic scattering, (n,2n), (n,d) and (n,n't) cross sections for ^{7}Li. These evaluated results for the (n,n't) reaction are in excellent agreement with the values of Smith et al. [9,10], and are also consistent with the data of Liskien and Paulsen [11], within the quoted errors. This evaluation was not excessively influenced by the results of Smith et al. [9,10] because of the constraints associated with the need to consistently fit a wide range of data for ^{7}Li reactions other than $^{7}Li(n,n't)^{4}He$. In fact, exclusion of the results of Smith et al. [9,10] produced a relatively small change in the evaluation [13]. The data of Swinhoe and Uttley [5,8] were thus found to be inconsistent with the general body of information on the dominant n + ^{7}Li cross sections. However, their suggestion in 1979 [5] that the $^{7}Li(n,n't)^{4}He$ cross section should be lowered relative to ENDF/B-IV [7] appears to be valid, though not to the extent that they suggested. The evaluation by Young [13] has been incorporated into ENDF/B-V [12] in a recent revision. In 1982, Liskien et al. [14] published the results of a $^{7}Li(n,n't)^{4}He$ experiment based on tritium activity measurements at Jülich. Their data cover the ranges ~ 5-8 MeV and ~ 13-16 MeV. The results in the lower-energy range tend to fall slightly lower by a few percent than the values of Smith et al. [9,10], but the agreement within quoted errors is very good. In the higher-energy range, the values of Liskien et al. [14] are noticeably lower than the evaluation of Young [13], though not as low as the values of Swinhoe and Uttley [5,8]. The history of this reaction prior to the present experiment,

as discussed in this paragraph, is summarized in Fig. 1. It appears that the knowledge of the cross section presently approaches the required accuracy of ~ 3% [1] in the 7-9 MeV range, but the uncertainties at ~ 14 MeV, and in the threshold region < 6 MeV, remain unacceptably large.

The objective of the present work was to perform a measurement of the $^{7}Li(n,n't)^{4}He$ reaction cross section in the vicinity of 14 MeV in order to try and resolve the discrepancy between the recent results of Liskien et al. [14] and the evaluation of Young [13] (ENDF/B-V [12], revised). The approach used in this experiment is similar to that reported previously by Smith et al. [9,10], except that a conventional DT 14-MeV neutron generator was employed for the neutron irradiations rather than the Argonne FNG accelerator [15]. Section II discusses the experimental procedure while Section III deals with the data analysis process. In both of these sections emphasis is placed on details which have not been documented in work previously published by this laboratory. In Section IV attention is given to the matter of errors, since quantitative reliability is an important objective of this work. The results of this experiment are presented, and compared with equivalent values from the literature, in Section V. The significance of the uncertainty in the ^{238}U neutron-fission cross section is also discussed. Details relating to our derivation of cross sections in the 14-MeV neutron field from the $T(d,n)^{4}He$ reaction are provided in the Appendix.

II. EXPERIMENTAL PROCEDURE

The basic method employed in this experiment was as follows: Wafers of ^{7}Li-enriched lithium metal, encapsulated in aluminum, were attached to a low-mass fission chamber containing a calibrated depleted-uranium deposit. The entire assembly was placed close to the target of a DT 14-MeV neutron generator for irradiation (as shown in Fig. 2). Tritium was extracted by vaporizing the samples and converting the released tritium, and hydrogen carrier gas, to water. The collected water samples were counted by the liquid-scintillation method to determine the tritium content of the lithium samples. The measured data were converted to $^{7}Li(n,n't)^{4}He$-to-^{238}U neutron-fission cross-section ratios, following the application of several corrections. The details of this procedure are discussed to varying degrees in the remainder of this section. Pertinent references to previous work from this laboratory are also provided.

A. Neutron Production

14-MeV-neutron production with DT-neutron generators is discussed extensively by Barschall [16]. In our experiment, a Texas Nuclear Generator Model No. 9400, operating at a nominal 150 ± 10 kV, was employed [17]. Deuterium-ion beams were extracted from an RF ion source which was supplied

from a deuterium-gas reservoir through a palladium leak. Typically, at ~ 150 kV, ~ 50-100 μA of accelerated-beam current could be obtained through a 1.27-cm diameter aperature placed in front of the neutron-producing target. The beams were undetermined mixtures of atomic (D^+) and molecular (D_2^+) ions. No components were available in the accelerator beam-transport line to permit unambiguous selection of the atomic component of the beam. However, the neutron-production cross section for the $T(d,n)^3He$ reaction increases rapidly with incident deuteron energy [16], reaching a peak at the well-known resonance ~ 110 keV. The neutron generator was adjusted to provide maximum neutron yield for a given beam current on target at ~ 150 kV, thus it is believed that most of the neutron production resulted from the ~ 150 keV D^+ atomic ions rather than from the ~ 75 keV deuterons bound in the D_2^+ molecular ions. The possible influence of the molecular component is discussed in some detail in Section III.

The neutron-producing targets were of the standard metal-tritide variety [16], and they were obtained commercially from Safety Light Corporation [18]. Tritium was absorbed in a host layer of Ti (~ 4 micrometers thick) on a 0.0254-cm-thick copper backing. Each target contained ~ 1 Ci/cm^2 when fresh. Since the range of ~ 150 keV deuterons is $\lesssim$ 1 micrometer in titanium, the incident deuterons were always stopped in the Ti-T layer. The initial abundances of T and Ti in this layer are roughly equal for such targets (e.g. Ref. 19), but some nonuniformity in relative density vs. depth into the layer is likely (e.g. Ref. 20). Furthermore, the yield from the targets is known to decrease with integrated beam dose (e.g., Ref. 16). This effect was very evident in the present experiment, with yields typically declining to ~ 20-30% of the initial yield after ~ 30 hours of continuous use. Investigation of the implications of target depletion was an important aspect of this experiment. Ti-T targets require adequate cooling to survive. The present targets were mounted in an air-cooled target assembly (as shown in Fig. 2). An air flow was directed along the back of the copper target disk to insure adequate cooling effectiveness. Three fresh Ti-T targets were used in this experiment. Each was discarded after accumulating ~ 5-6 Coulombs of integrated charge.

B. Lithium Samples and Fission Monitor

Isotopic ^7Li samples were prepared from 99.92%-pure lithium metal in the form of wafers 1.9-cm in diameter and roughly 0.6 cm thick. Each wafer was enclosed in an air-tight aluminum capsule with ~ 0.5 mm thick walls. These capsules prevented the lithium from reacting with the atmosphere (mainly with water vapor) and kept tritium from escaping, following irradiation. The samples had been fabricated ~ 4 y prior to this experiment. The weights prior to the experiment differed by < 0.1 mg from those recorded at the time of fabrication. Furthermore, each sample used passed two pressurized-helium leak tests (four years apart). These two indicators insured that no cladding failures were involved in this experiment. The ^7Li-enriched material (^7Li

to-^{6}Li ratio=1511) was obtained from the Stable Isotopes Division, Oak Ridge National Laboratory [21]. Table I from Ref. 9 gives specific information on this material (material No. ORNL 4731100). This reference also provides a detailed exposition of the sample fabrication process which, therefore, will not be repeated here. Four distinct samples were employed in the present work. Three were irradiated in independent exposures while a fourth unirradiated one helped to check the extraction/counting process for possible background and tritium contamination effects. Some additional properties of these samples are listed here in Table 1. During neutron irradiation, samples ^{7}Li#7 and ^{7}Li#24 were attached to the fission channels as shown in Fig. 2 while ^{7}Li#23 was oriented in reverse fashion. Some of the corrections differed for these two orientations, so a test of the correction precedures was provided.

The fission monitor is a low-mass, parallel-plate ionization flow chamber used to detect fission fragments emitted from a thin deposit of uranium (see Fig. 2). The chamber itself has 0.0254-cm-thick steel walls. The chamber electrode and uranium-deposit backing are 0.0254-cm-thick steel disks. Methane (CH_4) at atmospheric pressure forms the gaseous medium. The uranium deposit consists of a thin, uniform film of depleted uranium (effectively 100% ^{238}U) 2.54-cm in diameter, amounting to 4.988×10^{18} ($\pm$ 0.9%) atoms. Procedures for making and calibrating this deposit have been described previously [22-24]. The fission pulse-height signals were processed using a multichannel analyzer. The totality of events above a selected channel was recorded as the raw-fission-count data. This effective bias level was set in order to reject alpha-particle pulses, recoil proton events from neutron interaction with hydrogen in the methane gas, and electronic noise. Information required to calculate a correction for extrapolation of the fission spectrum to zero pulse height was also obtained for each run.

C. Irradiation Procedure

In addition to the fission events, the integrated beam charge and pulses from a long counter (LC) were recorded during each irradiation. The LC was mounted in a fixed position, and thus provided a stable monitor of neutron production from the Ti-T targets. A pulse ratemeter was also included in the LC circuitry to provide real-time information on the neutron yield for the purpose of adjusting the accelerator. The ratemeter was sampled every few minutes in order to provide records of all irradiations for later consideration during the data analysis process. Each lithium sample was irradiated for ~ 5-8 h per day during four consecutive days. These irradiations were interspersed with several shorter irradiations of Fe and Ni samples. The latter exposures were designed to provide information on the possible impact of deterioration of the Ti-T targets. A fresh Ti-T target was installed on the DT generator near the beginning of the sequence of irradiations for each lithium sample. Since only about four days elapsed between the start and finish of the irradiation sequence for each

sample (a negligible time interval when compared with the ~ 12 year T decay half life) no corrections were applied for exposure variations during the irradiation periods. The position of the fission detector and sample were such that the uranium deposit was ~ 5.3 cm from the neutron source while the samples were ~ 4.2-4.6 cm away. Both the ^{238}U-neutron-fission and ^{7}Li(n,n't)^{4}He processes exhibit threshold behavior so they were not expected to respond significantly to low-energy "room-return" neutrons. Nevertheless, measurements were made at various distances, in a different experiment which utilized the fission chamber alone, in order to test for departure from the anticipated "inverse-square law" behavior.

D. Tritium Extraction and Sample-Activity Measurements

The extraction of tritium from the lithium samples has been described in previous publications from this laboratory [9,10,25,26]. An isotopic-dilution method using normal hydrogen as the carrier gas is used. Fig. 3 is a schematic drawing of the extraction apparatus. The irradiated lithium sample (in its Al capsule) is placed in the chamber of a furnace. The system is evacuated and a precise quantity of ultra-pure (99.999%) hydrogen is added from a calibrated reservoir. The assembly is heated to a temperature high enough to melt the sample capsule and free the tritium from its chemical bonds to lithium (essentially LiT). The released T and H are passed through a freshly-activated CuO column where they are converted to water vapor. This vapor is collected in liquid-nitrogen cold traps, carefully weighed, and then sealed in glass ampules. Calculations are performed to determine how much of the hydrogen gas, introduced in the dilution method, is recovered in the water sample. Normally $\lesssim$ 6 grams of water are collected in a typical sample, and $\lesssim$ 1% of the hydrogen introduced into the system is lost. It is assumed that the recovery fraction for tritium is about the same as for hydrogen. This hypothesis has been tested extensively in this laboratory, and through intercomparison with other techniques (e.g., Refs. 10 and 26). The extraction apparatus was thoroughly cleaned prior to each extraction to minimize contamination problems. Furthermore, the lithium-sample extractions were interspersed with the generation of water samples from pure hydrogen alone (no lithium sample). Finally, the unirradiated sample, ^{7}Li#3, was also processed through this system as a control.

The activities of all the extracted water samples were determined by liquid-scintillation counting using a commercial facility [27]. The procedure is described in Refs. 10 and 26. Substandards for calibration of this facility were prepared from the NBS tritiated water standard SRM 4926-C [28]. The activity of the NBS standard is quoted as 3406 (± 0.63%) dps/g on September 3, 1978; however, this value has been revised upward by 0.7% to 3430 dps/g (with the same error) based on recent work at Rockwell International Corporation (Ref. 26). The counting efficiency of the present system was

determined to be 34.66 ± 0.10%. Furthermore, an average background count rate of 26.92 ± 0.27 cpm was measured for the counting system. All count data were corrected for this near-constant background. Table 2 summarizes the major parameters associated with the tritium extraction and counting procedures. Note that the calculated water-sample masses m(C), based on the carrier hydrogen introduced into the system and the measured sample masses m(E), differ by ~ 0.3-1.1%. The data were corrected for this effect. The negative values for dps/g H_2O associated with two of the background runs (no lithium) are not significant. For these measurements the observed count rates when the water samples were present are consistent with the ambient system counting background. The net dps/g H_2O should be treated as zero in each such instance. The fidelity of the entire tritium extraction and counting process has been tested, and intercompared between two laboratories, utilizing measurements for $^{6}Li(n,t)^{4}He$ alone, as discussed in Refs. 10 and 26.

The Fe and Ni samples, which were periodically irradiated in order to monitor possible effects of Ti-T target deterioration, were counted with a Ge(Li) detector. Absolute calibrations were not required since the information sought was the dependence of observed yields for the $^{56}Fe(n,p)^{56}Mn$, $^{58}Ni(n,p)^{58}Co$, $^{58}Ni(n,2n)^{57}Ni$ and ^{238}U neutron fission relative to each other and to the LC monitor. In order to obtain consistent results, the LC system had to be corrected for a deadtime factor which was determined experimentally.

III. DATA ANALYSIS

Reduction of the raw experimental data to cross-section ratios involved a combination of analytical and monte-carlo procedures. In addition to processing the data from the Li-sample irradiations, it was necessary to examine the Fe and Ni sample data carefully for indication of changes in the neutron spectrum during the course of the experiment.

A. Fission Data Processing

The fission pulses above a selected channel number were summed and corrected for multichannel-analyzer deadtime, an effect generally amounting to $\lesssim$ 0.1%. Extrapolation corrections were calculated for each run (four separate runs were performed for each sample) based on the assumption

of a flat spectrum at low pulse heights. The individual corrections were in the range 7.5-8.8%. Fission fragments emitted near 90° in the uranium deposit cannot escape and are thus not recorded. This effect is neutron-energy dependent, and it also depends upon the fragment angular distributions. The most significant dependence is upon the deposit thickness. Using fragment angular distribution data from Ref. 29, we determined that a correction of 2.7% was required. After these various corrections were applied to the raw-fissions data from the individual runs, the values pertaining to each particular lithium sample were summed, thereby yielding the integrated fission events per sample. A test for the consistency of the fission yield data through the course of the experiment was provided by examining the ratio of the corrected fissions to the deadtime-corrected LC monitor counts. The LC was, of course, mounted in a fixed position throughout the experiment, and the fission counter was very carefully placed the same distance from the target assembly for each run. Indeed, each individual ratio varied by $< 1\%$ from its corresponding tritium-target average, while various target averages differed by $\leq 0.5\%$ from the average of all three Ti-T targets. This consistency was achieved in spite of notable decline in the neutron output from the targets with elapsed time (e.g., see Fig. 4) and discernible differences in the yields from various Ti-T targets used in this experiment. While the LC is assumed to have only a relatively-gradual energy dependence for its efficiency, the ^{238}U neutron-fission cross section is known to change at a rate of + 8.2% per MeV of neutron-energy increase in this region, according to ENDF/B-V [12] (see Table 3). Although there was a slight tendency for the ratio of fissions to increase with target age (by $\lesssim 1\%$), the effect was small and served to support the contention that only minor changes occured in the neutron spectrum over the life of any target. This point is considered in detail later in this section.

B. Lithium-Sample Data Processing

The numbers of ^{7}Li atoms per sample were deduced from knowledge of the sample masses (Table 1), the ^{7}Li-to-^{6}Li isotope ratio (Section II) and the known mass of the ^{7}Li atom, 7.016005 a.m.u. [30]. The measured tritium activities were converted to total activated atoms per sample using the formula

$$N = d \cdot m \cdot \tau \cdot \exp(T_W/\tau) \quad , \qquad (1)$$

where d designates disintegrations per second per gram of lithium, m is the lithium sample mass, τ is the tritium decay mean lifetime, and T_W is the elapsed time between exposure and count. Values for m come from Table 1, and those for d are from Table 2. For each sample T_W was ≤ 158 days. The half life of tritium was taken to be 12.35 ± 0.04 y, an average of the 12.33 value from Lederer and Shirley [31] and a recent value of 12.38 y from Rockwell International Corporation [32]. Thus, the

correction for activity decay was $\leq$ 2.5% for each sample. These derived tritium-atom numbers were then corrected for contamination effects as follows: The data indicated in Table 2 are corrected for general counting background, so the background with which we are concerned here is of a different origin. Referring to Table 2, in the column labelled "dps/g H_2O", we notice significant differences in the values for BKG-1 through BKG-5, and for the placebo sample, ^{7}Li#3. For BKG-3 and -4, the values are consistent with zero. The observed variations are much larger than the errors in the measurements, with values of counts-per-second-per-sample from 0-0.35, compared with 0.45 counts per second for the constant counter background. We conclude, therefore, that the effect is due to a varying contamination associated with the extraction process. Since the value for the placebo sample is in the same range as the BKG-1 through BKG-5 extractions, we conclude that the effect has nothing to do with the virgin lithium material. One clue concerning the origin of this effect is discovered from the similarity of the contamination backgrounds for BKG-1 and BKG-5. These extractions involved use of the same furnace liner. In any event, the individual irradiated-sample count data were corrected using the corresponding BKG run (which was always made using the same liner). This led to a correction of zero for ^{7}Li#23 and ^{7}Li#24, and 1.2% for ^{7}Li#7.

C. Neutron Scattering Corrections

The production of fissions and tritium activity in this experiment was affected by neutron scattering from various laboratory structures, so corrections had to be determined. Contributors to this scattering effect were divided into two categories: i) components of the Ti-T target assembly and sample/fission detector arrangement which were close to the deuteron source, ii) everything else ("room return"). The scattering from the first category of components was assumed to be dominant, and monte-carlo calculations were performed to determine the magnitude of the effect. The basic concept is described in Ref. 33, but the calculational procedure has since been improved and it is further described in Ref. 34. The calculations involved only the additional events produced by singly-scattered neutrons. Elastic and inelastic scattering and (n,2n) processes were included. The latter process involves neutron multiplication which enhances the effect, nevertheless this process produced a smaller effect than the scattering channels. Table 4 indicates these scattering-correction contributions, identifying both origin and magnitude. Clearly the target structure is responsible for most of the scattering. The corrections largely cancel, however, resulting in a net effect of $\lesssim$ 1% on the measured ratio. The possibility of residual scattering effects not accounted for in the preceding calculations was investigated experimentally since calculation of such effects was considered impractical. Measurements were made at various distances from the neutron source using only the fission chamber and LC. The raw data recorded were fission-to-LC ratios. These data were corrected for

counter deadtime, geometry and the first category of neutron-scattering corrections indicated above. The resulting values were consistent with an "inverse-square law behavior, indicating that the "room-return" perturbations were negligible. In fact, at the ~ 5-cm distance of this experiment the "room-return" effect was found to be -0.06 ± 0.08% (the negative sign is nonphysical but that is not significant since the result is consistent with zero).

D. Cross-Section Calculations

The measured fission and tritium-activity data, and calculated corrections, were utilized to compute $^{7}Li(n,n't)^{4}He$-to-$^{238}U(n,f)$ cross-section ratios. The calculations were performed using the computer code ACTV14 described in the Appendix. This code determines a number of additional factors involving geometry, neutron source properties, neutron absorption, etc. The procedure is similar to that described in Refs. 33 and 35, refined to incorporate concepts described in Refs. 36 and 37. ACTV14 is an activation data processing code developed explicitly for measurements using Ti-T targets and the $T(d,n)^{4}He$ source reaction. Specific parameters for this source reaction which are required in the code were obtained from Liskien and Paulsen [38]. Specific energy loss information for deuterons in the Ti-T target was derived from Anderson and Ziegler [39]. Details are discussed in the Appendix. Auxillary cross section information, such as total cross sections for absorption analysis, the $^{238}U(n,f)$ cross section, and an a priori shape for $^{7}Li(n,n't)^{4}He$, were obtained from ENDF/B-V [12]. Various calculations were performed in order to examine the sensitivity of the results to variations in some of these input parameters. The calculations were totally insensitive to the assumed a priori $^{7}Li(n,n't)^{4}He$ cross section. Sensitivities to other parameters will be discussed later in this section and, along with consideration of the experimental errors, in Section IV. An advantage of this calculational procedure is that an effective neutron spectrum is also calculated. The particular spectrum resulting from the present experimental conditions is shown in Fig. 5. The average energy is 14.74 MeV with FWHM resolution of 0.324 MeV.

E. Investigation of Ti-T Target Aging Effects

As indicated previously, possible changes in the neutron spectrum with the age of the Ti-T target is a matter of concern since all measurements were performed in the vicinity of zero degrees where the spectrum is the most sensitive to these effects. The cross-section calculations performed with ACTV14 are based on the assumption that the tritium concentration is uniform with depth to well beyond the range of the deuterons. There are several reasons for suspecting a possible departure from this idealized representation [16]. Since explicit spectrum measurements were not made in this experiment, it was necessary to examine this effect indirectly, using the auxiliary measurements described in Section II. The decline in neutron

production from the targets must be due to one or more mechanisms which alter the concentration and/or distribution of tritium with depth into the Ti-T layer. Two extreme possibilities are envisioned: As one limit, we might assume that the decline in yield comes about solely as a result of an overall uniform decrease in tritium within the Ti-T layer, while uniformity of tritium concentration with depth is maintained. Then, the neutron spectrum shape would be unaltered. For the other limit, we could envision that tritium is preferentially depleted near the surface of the Ti-T layer. The decline in yield then comes about because the incident deuterons must transverse an increasingly-thick "dead" layer before impinging upon the tritium-bearing region. The average "effective" incident energy for the deuterons entering the tritium region drops and thus so does the neutron yield [16]. If one relies on Fig. IV.1 from Ref. 16, it is possible to derive an effective incident deuteron energy vs. target age. The effect on the derived $^{7}Li(n,n't)^{4}He$ cross section can be estimated using ACTV14. For each of the three Ti-T targets used in this experiment, the final target output was ~ 20-30% of the initial yield. Thus, the average incident deuteron energy over the irradiation period might be ~ 106 keV rather than 150 keV. This would imply an average incident neutron energy of ~ 14.65 MeV rather than 14.74 MeV, and a resolution of ~ 170 keV rather than 324 keV. In this limit, the $^{7}Li(n,n't)^{4}He$ cross section would decrease by only ~ 0.7%, indicating that the effect with which we are concerned is not of serious proportions in the present context. However, we pursued this matter in some detail in order to set limits on the uncertainty in the average neutron energy.

Using the data from the previously-mentioned Fe and Ni sample irradiations, and the fissions and LC data, eight spectral-indicator ratios were defined, and the variations of these with accumulated beam charge in the target were traced for each of three Ti-T targets used. The experimental data were least-squares fitted with straight lines representing ratio value vs. accumulated charge from zero to ~ 5 Coulombs. These data were generally quite consistent with an assumed linear model, and the derived slopes were small. Slope values for the ratios considered are given in Table 5. Also given are the neutron-energy sensitivities of these indicators, based on data in Table 3 which was obtained from ENDF/B-V [12]. Using these sensitivities, it is possible to calculate the apparent neutron energy shift with target age. These results also appear in Table 5. The shifts are not large and they indicate no clear trend. The average of all the shifts is +3 keV. If only the ratios involving the LC counter are considered, the average shift is -6 keV with 39 keV uncertainty. However, the energy dependence of the LC response was not measured, and is only assumed to be nearly flat from 14-15 MeV. Consequently, the reaction-ratio spectral indicators are probably more reliable. For these, the average shift is again +3 keV with 24 keV uncertainty. Based on these findings, we decided that the uniform depletion model mentioned above is a closer representation of reality than the surface-depletion model. Consequently we chose to accept the cross section values based on ACTV14 calculations with ~ 150 keV average deuteron energy, and applied no corrections for energy shift.

Deuteron buildup in the Ti-T targets with prolonged usage could lead to an alteration of the spectrum due to neutrons produced from the $D(d,n)^3He$ reaction. If the deuteron beam is predominantly atomic, this would not be a serious problem since the deuterium would tend to accumulate near the end of the deuteron range where the average incident energy is low. If a significant molecular component is present, then deuterium would also accumulate near midrange for the atomic beam and a problem could develop. In previous tests with blank (no tritium) targets, a buildup in neutron yield with accumulated deuteron-beam change had been observed, although the intensity was very small when compared with a Ti-T target. The reaction-ratio spectral indicators provide a means for examining this effect. We could choose to interpret any change in these ratios with accumulated deuteron charge Q as originating from ~ 2.5-MeV $D(d,n)^3He$ neutrons. Here a represents the rate of deuterium buildup in the target, R is the ratio Y/Y_m, where Y represents the numerator reaction yields and Y_m the demoninator reaction yields from Table 6, and σ and σ_m are the corresponding reaction cross sections, respectively, then

$$R_Q \approx R_0 \{1 + aQ [\sigma(2.5)/\sigma(14.7) - \sigma_m(2.5)/\sigma_m(14.7)\} \quad , \qquad (2)$$

provided that $[aQ\sigma_m(2.5)/\sigma_m(14.7)] \ll 1$. Table 6 summarizes the results of this interpretation of the spectral-indicator results. It is seen that the deuterium buildup effect is ~ 0.5% with an error of 0.7%, i.e., effectively insignificant. No corrections were applied to the data for this effect.

F. Miscellaneous Effects and Corrections

Several other effects not treated in the analysis prior to and including the ACTV14 calculations were considered next, and corrections were applied where warranted. In ACTV14, the net effect of neutron absorption by the Aℓ sample cladding was calculated by assuming a 0.0508-cm layer of Aℓ between the sample and uranium deposit, in addition to the 0.0508-cm Fe wall of the fission detector (see Fig. 2). This is an oversimplification which ignores edge effects and other complexities of the capsule structure. Closer consideration of the neutron absorption effects led to a correction of 1.5% for samples ^{7}Li#7 and ^{7}Li#24 and 1% for ^{7}Li#23. The possibility of tritium production from Aℓ(n,t) reactions in the sample cladding was considered. This effect was previously found to be negligible at lower energies (Ref. 9), and based on cross section data from Refs. 40-44 we conclude that the effect is also negligible in the 14-15 MeV range. In code ACTV14, no provision is made to accommodate a neutron source with finite lateral extent. In fact, the neutron source is essentially a disk with ~ 1.27 cm diameter. Over the relatively-small angular ranges extended by the sample and uranium deposit, the neutron source is nearly isotropic [38]. Numerical calculations were performed on a digital computer to simulate the finite extent of the source, assuming isotropy, and it was found that effects on both the fission and tritium activity results fall in the range 1-2%. The net effect on the ratio, however, is $\ll$ 1% so no corrections were applied to the measured results. Tritium produced in the lithium tends to remain bound in the material as LiT. Since, in

fact, none of the samples used in this experiment showed any signs of leakage, possible loss of tritium due to leakage was therefore considered negligible. The possibility of penetration by energetic tritons through the capsule walls was also eliminated from consideration since the range of the tritons was always < 0.03 cm while the Al cladding was > 0.05 cm in thickness. Finally, the effect of $^{6}Li(n,t)^{4}He$ reactions, shown in Ref. 9 to be negligible for the 7-9 MeV range, was also neglected here as well since the ^{6}Li-to-^{7}Li tritium-production cross section ratio is even smaller at ~ 14 MeV than at the lower energies previously considered.

IV. EXPERIMENTAL ERRORS

The sources of error considered in the present work are summarized in Table 7. The random errors apply independently to the cross-section values derived from the three different irradiated Li samples, while the systematic errors apply identically to each of them and are fully correlated (100%). Some of the error sources considered appear to be negligible. Others are obvious and so require no further discussion.

First we consider the random errors. The tritium recovery losses were estimated by comparing m(C) with m(E) for the derived water samples, as discussed in Section II. Each extraction was an independent process. While the observed differences may be real, we conservatively assume that the scatter of m(C)-to-m(E) ratio values, from Table 2, are statistical and thus deduce the 0.4% error from the variance. The counting-facility general background of 26.92 ± 0.27 cpm produced an uncertainty in the measured tritium actvities of < 0.1%, so an error of 0.1% conservatively covers this effect. For two of the samples, the contamination effect was observed to be negligible. For the third, a 1.2% correction was applied. The uncertainty in this correction was ~ 15%, leading to ~ 0.2% uncertainty in the final results. The cross sections calculated by ACTV14 are somewhat sensitive to distance since the Li and U deposit are not exactly superimposed. We estimated a random error of $\lesssim$ 0.5 mm in this distance, and thus ~ 0.2% error in the cross section.

Systematic error in the tritium decay half life affects the cross section directly via Eq. (1). The uncertainty of ~ 0.3% is based on the spread between the half life values of Refs. 31 and 32. The ~ 0.6% error in the NBS tritiated water standard is that quoted by NBS [28]. The error of 0.3% in calibration of the tritium counting facility represents all calibration errors other than that for the water standard. The ^{238}U deposit was standardized by a fission-ratio measurement at 2.5 MeV relative to a standard ^{235}U deposit. The uncertainty in the measured ratio is ~ 0.8% (per Ref. 45) while the uncertainty in the mass of the ^{235}U deposit is 0.3% (per Ref. 46). The combined error of ~ 0.9% is taken to be the error in the derived ^{238}U

deposit mass. A systematic uncertainty in the extrapolation correction exists because of a lack of explicit knowledge of the proper shape for the extrapolated spectra. We assume an error of 20% in the correction and thus have a 1.6% error in the derived cross sections. Likewise a 20% systematic error is assumed in the thickness correction which leads to ~ 0.5% error in the cross section. In Section III it was indicated that tests of the "inverse-square law" dependence of fission events confirmed this behavior to within $\lesssim$ 0.1% so no corrections were applied. Arbitrarily we chose to assign an error of ~ 0.1% to cover this effect. Most of the error due to the neutron absorption corrections is related to modeling the edge effects in the Al-clad lithium samples. The magnitude of this error is estimated at ~ 0.3%. The multiple-scattering corrections largely cancel; however, we assume an error of ~ 30% in the net correction of 0.9%, which amounts to an error of ~ 0.3% in the cross section. Based on the spectral-indicator measurements, it appears that the average effective incident deuteron energy for tritium production is relatively unchanged over the course of a measurement. The neutron generator potential is 150 ± 10 kV, and neutron production is apparently largely produced by atomic-deuteron beams. The uncertainty in the average neutron energy is therefore ~ 20 keV, with a resulting uncertainty in the cross section ratio of ~ 0.1%. Finally, we estimated ~ 0.2% systematic error for geometric effects, primarily those due to imperfect knowledge of the absolute distance from the Ti-T target to the Li-sample/fission detector combination (Fig. 2).

The error in the ^{238}U neutron-fission standard cross section should be considered separately from the errors affecting the measured ratios. The error in this cross section does not affect the accuracy of our measured ratios, but it does have a strong influence on the accuracy which we can expect for the derived $^{7}Li(n,n't)^{4}He$ cross section. According to ENDF/B-V, the error in the $^{238}U(n,f)$ cross section for the 14-20 MeV region is 6.4% [12]. The origin of this evaluation was the work of Poenitz et al. [47]. In this work it was suggested that the error is 4.3% at 14 MeV and 8.5% at 20 MeV. Obviously the 6.4% selected for ENDF/B-V [12] is an average of the limiting errors at the group boundaries. We suspect that for 14.74 MeV, the error should be smaller than 6.4%, so we assume a linear variation of the error from 4.3 to 8.5% across the group. With this assumption, the $^{238}U(n,f)$ cross section error at 14.74 MeV amounts to 4.8%, so this is the value we selected to use rather than 6.4%.

V. RESULTS AND CONCLUSIONS

The principal results for this experiment are summarized in Table 8. The ratios measured for the three different Li samples agree very well within the quoted random errors. Therefore, it is reasonable to average

them using inverse-square random errors for weighting factors, as described in Ref. 48. The resulting weighted-average ratio bears a random error of only ~ 0.5% compared with the individual ratio errors which are closer to ~ 1%. The systematic error is unaffected by the averaging procedure.

The final cross section of 0.301 (± 5.3%)barn for the $^{7}Li(n,n't)^{4}He$ reaction is compared with corresponding measured and evaluated results for the 12-17 MeV energy range in Fig. 6. The present result is ~ 3% higher than the evaluated value of Young [13]. This is excellent agreement considering that the experimental error for the present result is ~ 5% and the uncertainty in the evaluated value is ~ 4-5% at this energy. The results of Liskien et al. [14] are ~ 10% lower than the evaluation of Young, and thus are ~ 13% lower than our result. This difference exceeds the combined errors of the measurements (~ 6-7% for the values of Liskien et al. [14]). The values of Swinhoe and Uttley [5,8] fall considerably below any of the above-mentioned results.

In general, the data base for neutron interaction with ^{7}Li is relatively sparse and uncertain above ~ 14 MeV, and this is reflected in the errors quoted in the evaluation by Young [13]. Consequently, any revised evaluation, which should include the present $^{7}Li(n,n't)^{4}He$ cross section value, would very likely be strongly influenced by it. The present experiment fails to achieve the desired 3% accuracy objective solely because of the uncertainty associated with the ^{238}U neutron-fission cross section which we are using as a standard. The ratio measurement reported here is quite accurate (~ 2.2%), and the 3% objective would be achieved if the standard cross section were known to ~ 2% accuracy. Prior to any re-evaluation of the $^{7}Li(n,n't)^{4}He$ cross section, it seems to be necessary to improve the knowledge of the ^{238}U neutron-fission cross section over the 14-15 MeV energy range, from the current ~ 5% uncertainty level to an accuracy of ~ 2%. This objective is not a trivial one, but achieving it should be feasible utilizing existing methods. As is usual in seeking accuracies at this level, measurements should be performed at more than one laboratory and several methods ought to be pursued.

ACKNOWLEDGEMENTS

This work was supported by the U.S. Department of Energy. The encapsulated lithium samples were fabricated by R. Hopf. D. Bowers assisted with the tritium activity measurements. The ^{7}Li-to-^{6}Li isotope ratio determinations at Argonne were performed by E. Callis and A. Essling.

APPENDIX

The methods used in this laboratory to calculate activation-reaction cross sections have been described in previous publications. Analysis for measurements with the $^{7}Li(p,n)^{7}Be$ source is described in Ref. 33. Details relevant to the $D(d,n)^{3}He$ source (with a gas target) are discussed in Ref. 35. The technique used to calculate the effective neutron spectrum is describe in Ref. 36, and is also mentioned in Ref. 37. Here we outline some of the procedures involved when the neutron source is the $T(d,n)^{4}He$ reaction, with relatively low-energy deuterons from a DT 14-MeV neutron generator incident upon titanium-tritide (Ti-T) targets.

Fig. 7 is a schematic diagram which shows those components of the apparatus in Fig. 2 which are essential in the calculation. The neutron target is assumed to be a point. The longitudinal extent is indeed quite negligible (~ 1 micrometer), however the lateral extent is not since it is actually a circular region with diameters typically in the range 1-2 cm. Considerable simplification in the analysis is achieved if this lateral extent is neglected. The corrections required due to this neglect turn out to be quite small in most cases of interest (e.g., in the present experiment as discussed in Section III), and they can be readily calculated separately to the desired accuracy, as required. We assume that tritium is uniformly distributed in a lattice of Ti. The relative concentrations of tritium and Ti are not important for the present purposes, although typically the concentrations are about equal in a fresh target (e.g., Ref. 19). Mono-energetic deuterons from the 14-MeV generator penetrate into the Ti-T layer, losing energy along the way, and stop before reaching the limits of the layer. We envision dividing the deuteron range into several equal increments Δx. The relative neutron yield from the i^{th} increment is given by

$$\Delta F(x_i,\theta) \sim \Delta x\ \sigma_{DT}(E_{di},\theta) \quad , \tag{3}$$

where x_i is the midpoint of the i^{th} path increment, E_{di} designates the deuteron energy at that point of the path, θ is the angle of neutron emission and σ_{DT} is the DT-neutron-production cross section. Unimportant proportionality constants are omitted from Eq. (3). We have no specific interest in the yield per increment of path range, so we convert Eq. (3) to the form

$$\Delta F(E_{di},\theta) \sim \Delta E_{di}\ \sigma_{DT}(E_{di},\theta)/S(E_{di}) \quad . \tag{4}$$

Extensive tables of $\sigma_{DT}(E_{di},\theta)$ are available in Liskien and Paulsen [38]. $S(E_{di})$ is the stopping power of the material along the deuteron

path. Stopping power information is available from Anderson and Ziegler [39], but some consideration needs to be given to how this particular information is used. We choose to assume that the stopping power is dominated by titanium. Since the electrons in the material are responsible for slowing down heavy particles, and most of the electrons come from the titanium atoms, this appears to be a reasonable assumption for the Ti-T layer. Stopping power values in Ref. 39 are given for protons vs. (E/m), with abscissa units of keV per amu. When utilizing this tabulated information we must realize that the stopping power for a deuteron of energy E_d is approximately equal to that for protons of energy 0.5 E_d. This approximation is quite good at energies well above the Bragg peak (energies >> 100 keV) but is not so good at lower energies where shell effects and other factors lead to more complicated relations than the Bethe formula for stopping power. In spite of this, we choose to apply these approximations at all energies and remark here that the results turn out to be relatively insensitive to the shape of the stopping power curve.

If Y_F and Y_S are corrected fission and sample activated-atom yields, respectively, and the geometric parameters are as shown in Fig. 7, we obtain the expressions

$$Y_F \sim M_F \sum_{ij} [\sigma_{DT}(E_{di},\theta_{Fj})/S(E_{di})]\eta_{Fj}(A_{Fj}/\pi R_F^2)N_U\sigma_F(E_{nFij})/\ell_{Fj}^2, \tag{5}$$

and

$$Y_S \sim M_S \sum_{ijk} [\sigma_{DT}(E_{di},\theta_{Sjk})/S(E_{di})]\eta_{Sjk}\,(V_{Sjk}/\pi R_S^2 T_S)N_S\sigma_S(E_{nSijk})/\ell_{Sjk}^2. \tag{6}$$

Proportionality constants which cancel are omitted from these equations. Here M_F and M_S represent multiple-scattering corrections, η_F and η_S are neutron absorption factors, A_{Fj} is an element of uranium-deposit area, V_{Sjk} is an element of sample volume, $\sigma_F(E_{nF})$ is the fission cross section at neutron energy E_{nf} and $\sigma_S(E_{nS})$ is the activation cross section at neutron energy E_{nS}. Ultimately, Eqs. (5) and (6) can be used to derive an expression for the desired cross-section ratio at the average energy of the neutron spectrum. The form is essentially

$$R_m = C\ Y_S/Y_F. \tag{7}$$

The factor C is calculated using a computer code designated as ACTV14. In fact, this code does several other things as well: It calculates the actual neutron spectrum shapes for both the fission and activations channels, and yields the average neutron energies. The explicit spectrum-average cross section for activation in the 14-MeV spectrum is deduced, and this in turn is converted to a point cross section at the average neutron energy of the spectrum (usually they are nearly identical). This cross section calculation uses the energy-dependent standard-reaction (fission) cross sections which form part of the input data. In this analysis it is assumed that only one

fissioning isotope is present in the uranium deposit, namely ^{238}U.

Code ACTV14 is written in FORTRAN, and can be run on a relatively small computer. A listing of the code source appears at the end of this Appendix, along with input and output for a sample problem.

Next, we define the input and output parameters of code ACTV14. The reader is referred to the source listing and sample problem material for format information:

ACTV14 Input Parameters

(IRD, IWR, IPN)

These are program-control parameters which are entered from the computer console (Unit 4).

IRD = Unit number for primary input device, e.g., a card reader.

IWR = Unit number for primary output device, e.g, a printer.

IPN = Unit number for auxiliary output device used to record sample activity profile.

NOTE: If desired, the relative number of activated atoms in each cell of the sample can be provided. This is useful for the examination of any effects which nonuniform sample activity may have on some counting operations. Setting IPN=0 suppresses this output.

(IC)

This is a flag which indicates the nature of the operations to be executed next by the computer.

IC = 1 Pause and return to control section upon resumption of execution.

IC = 2 A complete set of input data is to be read.

IC = 3 A partial set of input data is to be read, and current values in the computer memory are used for the remaining parameters.

All of the following parameters are read when IC=2:

(N238)

Designates the number of energy (MeV)-cross section (b) pairs for the

standard-reaction cross section table. Presumably a fission reaction is employed. Cross section values are deduced by linear interpolation of this table.

(E238(I), SIG238(I), I=1, N238).

Energy and cross section table for the standard reaction.

(NSTM)

Designates the number of energy (MeV)-macroscopic cross section (cm^{-1}) pairs for the sample total-cross section table.

(ESTM(I), SIGTM(I), I=1, NSTM)

Energy and macroscopic cross section table for the sample total cross section.

(NSTBM)

Designates the number of energy (MeV)-macroscopic cross section (cm^{-1}) pairs for backing material located between the sample and uranium deposit.

(ESTBM(I), SIGTBM(I), I=1, NSTBM).

Energy and macroscopic cross section table for sample-backing total cross section.

The two preceding cross section sets are employed in ACTV14 for neutron absorption calculations. If the absorbers are compounds or have more than one layer (such as the Al-clad Li samples in the present work) this can be handled in part by constructing suitable macroscopic cross section tables.

(NSIGR)

Designates the number of energy (MeV)-cross section (only relative shape vs. energy is required) pairs for the sample-activation cross section.

(ESIGR(I), SIGR(I), I=1, NSIGR)

Energy and cross section table for the sample-activation cross section.

NOTE: This information is used in ACTV14 to calculate a factor which converts from spectrum-average cross section to a point cross section at the average neutron energy for the spectrum. This correction factor is usually quite small and essentially vanishes if the shape of the activaton cross secton is nearly linear over the energy range of the spectrum. If this is the case, then a constant cross section can be assumed without loss of accuracy in the ACTV14 calculations (see Ref. 36).

(NEDT)

Designates the number of deuteron-energy (MeV) grid points used in representing the $T(d,n)^4He$ neutron source.

(EDT(I), I=1, NDT)

Deuteron-energy grid values.

(NTHDT)

Designates the number of neutron-emission-angle (radians) mesh points used in representing the $T(d,n)^4He$ neutron source.

(THDT(I), I=1, NTHDT)

Neutron-emission-angle grid values. Emission angles are in the range $(0,\pi)$.

[(SIGDT (I,J),I=1, NEDT), J=1, NTHDT]

Neutron emission cross section values, vs. deuteron energy and neutron-emission angle. Only shape information is required. Values from Ref. 38 are used in the present work.

(NSTI)

Designates the number of deuteron energy (MeV)-stopping power (only relative values are required) pairs for the stopping power table applicable to deuterons in the Ti-T layer.

(ESTI(I), STI(I), I=1, NSTI)

Deuteron energy and stopping power table for deuterons in Ti-T. Values used in the present work are derived from Ref. 39.

When IC=3 only the following parameters are read:

(LABEL(I), I=1, 40)

80-column user-selected BCD label for calculational problem.

(NT,NRF,NRS,NHS,NP)

Mesh parameters for ACTV14 calculations.

NT = number of equal-energy increments into which the incident deuteron energy is subdivided for target-neutron-yield calculations.

NRF = radial mesh for uranium deposit.

NRS = radial mesh for sample.

NHS = thickness mesh for sample.

NOTE: The uranium deposit is so thin that it is treated as a single non-absorbing film of negligible thickness.

NP = profile mesh for representing the effective neutron spectra for producing fissions and sample activations.

NOTE: The neutrons are not monoenergetic because of deuteron energy loss in the Ti-T target and kinematic effects. The spectra which are calculated are those which would produce the observed fission and activation yields for a hypothetical calculational model in which the uranium and sample materials are compressed to a point, with all absorption effects suppressed.

Development tests of code ACTV14 indicated that the choice NT=NRF=NRS=50, NHS=10 and NP=30 provides acceptable accuracy with reasonable computation times. Little is gained by using finer mesh selections. Coarser meshes can be used to speed up the computations, but some sacrifice of accuracy may result.

(RF)

Radius of uranium deposit (cm).

(XB)

Spacing between sample and uranium deposit (cm).

(EDIN)

Incident deuteron energy from the 14-MeV generator (MeV).

ACTV14 Output Parameters

Some of the output is a repeat of the input and does not need further definition.

(ENAV)

Average neutron energy for the sample (MeV).

(DEMAXS)

Maximum neutron-energy spread for the sample (MeV).

(SRMEAS)

Spectrum-average activation cross section (b).

(FACTK)

Factor converting spectrum-average activation cross section to a point cross section at ENAV.

(SRCEAV)

Point activation cross section at ENAV (b).

(ENFAV)

Average neutron energy for the uranium deposit (MeV).

(DEMAXF)

Maximum neutron-energy spread for the uranium deposit (MeV).

(DF)

Distance from neutron source (a point) to the uranium deposit (cm).

(ATU238)

Absolute number of atoms in the uranium deposit which produce the observed fissions. A single isotope is assumed.

(YF)

Total observed fissions, corrected for all perturbing effects.

(VMF)

Multiple-scattering correction factor for the fission events.

NOTE: VMF $\geq$ 1 always.

(RS)

Sample radius (cm).

(HS)

Sample thickness (cm).

(DN)

Distance from neutron source to front of the sample (cm).

(ATS)

Absolute number of atoms in the sample participating in the production of the activity under consideration.

(YS)

Absolute number of atoms activated during the irradiation, corrected for all perturbing effects.

(VMS)

Multiple-scattering correction factor for the sample activations.

NOTE: VMS $\geq$ 1 always.

(V238AV)

Cross section for the standard reaction (fission) at ENFAV.

The format of the neutron-spectrum output is semi-graphical in nature, and is essentially self explanatory. The format of the output information on unit IPN is easily inferred from the source listing of ACTV14. The values YSUM(IRS,IHS) are relative concentrations of activity in each cell of the sample, corresponding to the sample radial (IRS) and axial (IHS) cell indices.

During developmental testing of ACTV14, the sensitivity of the calculated results to the assumed shape of the Ti-T target stopping power was investigated. It was found that if the Ti stopping power curve was replaced with a constant stopping power, there were only rather small changes in the computed results, e.g., the average neutron energy changed by < 10 keV and the computed $^{7}Li(n,n't)^{4}He$ cross section changed by $< 0.1\%$.

```
*JOB
*REW,17
*K,I05,L09,P17
*FTN
 OPT LXPC
       PROGRAM ACTV14
C      ACTV14 - D.L. SMITH - CDC 1700 - X2-6021 (314-109)
C
       COMMON E238(200),SIG238(200),EDT(25),THDT(25),SIGDT(25,25),ESTI(25
      1),STI(25),ESTM(200),SIGTM(200),ESTBM(200),SIGTBM(200),ESIGR(200),S
      2IGR(200)
       COMMON LABEL(40),EPF(50),PF(50),EPS(50),PS(50),KIF(21),KIS(21),YSU
      1MS(50,10)
C
       DATA PI,ISTAR,IBLANK,IDASH/3.14159,1H*,1H ,1H-/
C
       VALUE(IV,NV,VMAX,VMIN)=VMIN+((VMAX-VMIN)*(FLOAT(IV)-0.5)/FLOAT(NV)
      1)
       VINT(XL,XH,VL,VH,X)=VL+(X-XL)*(VH-VL)/(XH-XL)
C
C      INITIALIZATION AND CONTROL
C
 1000 WRITE(4,1001)
 1001 FORMAT(/6HACTV14)
      WRITE(4,1002)
 1002 FORMAT(/11HI/O DEVICES)
      WRITE(4,1003)
 1003 FORMAT(35HINPUT-IRD,PRINT-IWR,PUNCH-IPN (3I2)/)
      READ(4,1004) IRD,IWR,IPN
 1004 FORMAT(3I2)
    1 READ(IRD,2) IC
    2 FORMAT(I1)
      GO TO(10,20,30),IC
   10 PAUSE
      GO TO 1000
C
C      READ INTERPOLATION TABLES ON UNIT IRD
C
   20 READ(IRD,21) N238
   21 FORMAT(16I5)
      READ(IRD,22) (E238(I),SIG238(I),I=1,N238)
   22 FORMAT(8E10.4)
      READ(IRD,21) NSTM
      READ(IRD,22) (ESTM(I),SIGTM(I),I=1,NSTM)
      READ(IRD,21) NSTBM
      READ(IRD,22) (ESTBM(I),SIGTBM(I),I=1,NSTBM)
      READ(IRD,21) NSIGR
      READ(IRD,22) (ESIGR(I),SIGR(I),I=1,NSIGR)
      READ(IRD,21) NEDT
      READ(IRD,22) (EDT(I),I=1,NEDT)
      READ(IRD,21) NTHDT
      READ(IRD,22) (THDT(I),I=1,NTHDT)
      DO 23 J=1,NTHDT
   23 READ(IRD,22) (SIGDT(I,J),I=1,NEDT)
      READ(IRD,21) NSTI
      READ(IRD,22) (ESTI(I),STI(I),I=1,NSTI)
C
C      READ VARIABLE PARAMETERS ON UNIT IRD
C
   30 READ(IRD,31) (LABEL(I),I=1,40)
   31 FORMAT(40A2)
```

```
      READ(IRD,21) NT,NRF,NRS,NHS,NP
      READ(IRD,22) RF,XB,DF,ATU238,YF,VMF
      READ(IRD,22) RS,HS,DN,ATS,YS,VMS
      READ(IRD,22) EDIN
C
C     PRELIMINARIES
C
      SUMF=0.0
      SUMSP=0.0
      SUMEN1=0.0
      SUMD1=0.0
      SUMK=0.0
      DO 410 IP=1,NP
  410 PS(IP)=0.0
      SMEN1F=0.0
      SUMD1F=0.0
      DO 411 IP=1,NP
  411 PF(IP)=0.0
      DO 412 IRS=1,NRS
      DO 412 IHS=1,NHS
  412 YSUMS(IRS,IHS)=0.0
      THF1=ATAN(RS/DN)
      THF2=ATAN(RS/(DN+HS))
C
C     CALCULATE MAXIMUM DEUTERON ENERGY RANGE. AVOID ZERO FOR LOWEST
C     ENERGY TO PREVENT PROBLEMS WITH SUBROUTINE KINAM
C
      DED=EDIN-0.001
C
C     CALCULATE MAXIMUM NEUTRON ENERGY SPREAD
C
      THMAX=ATAN(RS/DN)
      CALL KINAM(2.0141,3.0160,1.00866,17.590,EDIN-DED,THMAX,EN1MIN,EDM)
      CALL KINAM(2.0141,3.0160,1.00866,17.590,EDIN,0.0,EN1MAX,EDM)
      DEMAXS=EN1MAX-EN1MIN
      DO 444 IP=1,NP
  444 EPS(IP)=DEMAXS*FLOAT(IP)/FLOAT(NP)
      THMAXF=ATAN(RF/DF)
      CALL KINAM(2.0141,3.0160,1.00866,17.590,EDIN-DED,THMAXF,EN1MF,EDM)
      DEMAXF=EN1MAX-EN1MF
      DO 445 IP=1,NP
  445 EPF(IP)=DEMAXF*FLOAT(IP)/FLOAT(NP)
C
C.....START OF TARGET LAYER LOOP
C
      DO 8888 IT=1,NT
C
C     CALCULATE ED AND VSTI AND DEDUCE IS
C
      ED=VALUE(IT,NT,EDIN,EDIN-DED)
      CALL INTRPL(NSTI,ESTI,STI,ED,VSTI,INDEX)
      IF(INDEX.EQ.0) GO TO 10
      CALL FINDI(NEDT,EDT,ED,IS,INDEX)
      IF(INDEX.EQ.0) GO TO 10
C
C000  COMPUTE CONTRIBUTIONS TO FISSION DEPOSIT SUM
C
      DO 70 IRF=1,NRF
C
C     GEOMETRY
C
      RFV=VALUE(IRF,NRF,RF,0.0)
```

```
      DFV2=RFV*RFV+DF*DF
      THF=ATAN(RFV/DF)
C
C     COMPUTE NEUTRON ENERGY, FLUX AND ATTENUATION
C
      CALL KINAM(2.0141,3.0160,1.00866,17.590,ED,THF,EN,EDM)
      CALL FINDI(NTHDT,THDT,THF,LS,INDEX)
      IF(INDEX.EQ.0) GO TO 10
      A=VINT(EDT(IS),EDT(IS+1),SIGDT(IS,LS),SIGDT(IS+1,LS),ED)
      B=VINT(EDT(IS),EDT(IS+1),SIGDT(IS,LS+1),SIGDT(IS+1,LS+1),ED)
      VSIGDT=VINT(THDT(LS),THDT(LS+1),A,B,THF)
      FLUX=VSIGDT/VSTI
      CALL INTRPL(NSTM,ESTM,SIGTM,EN,VSTM,INDEX)
      IF(INDEX.EQ.0) GO TO 10
      CALL INTRPL(NSTBM,ESTBM,SIGTBM,EN,VSTBM,INDEX)
      IF(INDEX.EQ.0) GO TO 10
      PATHBF=XB/COS(THF)
      IF(THF.LE.THF2) PATHSF=HS/COS(THF)
      IF(THF.GE.THF1) PATHSF=0.0
      IF(THF.GT.THF2.AND.THF.LT.THF1) PATHSF=(RS/SIN(THF))-(DN/COS(THF))
      ATTNF=EXF(-PATHSF*VSTM-PATHBF*VSTBM)
C
C     COMPUTE URANIUM DEPOSIT MACROSCOPIC CROSS SECTION
C
      CALL INTRPL(N238,E238,SIG238,EN,VS238,INDEX)
      IF(INDEX.EQ.0) GO TO 10
      SIGFM=ATU238*VS238
C
C     UPDATE FISSION DETECTOR SUMS
C
      QF=ATTNF*FLUX*RFV/DFV2
      SUMF=SUMF+QF*SIGFM
      SMEN1F=SMEN1F+EN*QF
      SUMD1F=SUMD1F+QF
      DENF=EN-EN1MF
      CALL SELECI(EPF,NP,DENF,JEF)
      PF(JEF)=PF(JEF)+QF
C
   70 CONTINUE
C
C000  END FISSION DETECTOR LOOP
C
C-----COMPUTE CONTRIBUTIONS TO SAMPLE SUMS
C
C     GEOMETRY
C
      DO 99 IHS=1,NHS
      XSV=VALUE(IHS,NHS,HS,0.0)
C
      DO 99 IRS=1,NRS
      RSV=VALUE(IRS,NRS,RS,0.0)
      DNSV=DN+XSV
      THS=ATAN(RSV/DNSV)
      PATHSS=XSV/COS(THS)
      DSV2=RSV*RSV+DNSV*DNSV
C
C     COMPUTE NEUTRON ENERGY, FLUX AND ATTENUATION
C
      CALL KINAM(2.0141,3.0160,1.00866,17.590,ED,THS,EN,EDM)
      CALL FINDI(NTHDT,THDT,THS,LS,INDEX)
      IF(INDEX.EQ.0) GO TO 10
      A=VINT(EDT(IS),EDT(IS+1),SIGDT(IS,LS),SIGDT(IS+1,LS),ED)
```

```
      B=VINT(EDT(IS),EDT(IS+1),SIGDT(IS,LS+1),SIGDT(IS+1,LS+1),ED)
      VSIGDT=VINT(THDT(LS),THDT(LS+1),A,B,THS)
      FLUX=VSIGDT/VSTI
      CALL INTRPL(NSTM,ESTM,SIGTM,EN,VSTM,INDEX)
      IF(INDEX.EQ.0) GO TO 10
      ATTNS=EXF(-VSTM*PATHSS)
C
C     COMPUTE ACTIVATION CROSS SECTION FROM TRIAL INPUT
C
      CALL INTRPL(NSIGR,ESIGR,SIGR,EN,VSIGR,INDEX)
      IF(INDEX.EQ.0) GO TO 10
C
C     UPDATE SAMPLE SUMS
C
      QUAN=ATTNS*FLUX*RSV/DSV2
      YSUMS(IRS,IHS)=YSUMS(IRS,IHS)+QUAN*VSIGR
      SUMSP=SUMSP+QUAN
      SUMEN1=SUMEN1+EN*QUAN
      SUMD1=SUMD1+QUAN
      SUMK=SUMK+VSIGR*QUAN
      DENS=EN-EN1MIN
      CALL SELECI(EPS,NP,DENS,JES)
      PS(JES)=PS(JES)+QUAN
C
   99 CONTINUE
C
C-----END SAMPLE LOOP
C
 8888 CONTINUE
C
C.....END TARGET LOOP
C
C     COMPUTE AVERAGE NEUTRON ENERGIES FOR BOTH THE MONITOR AND
C     THE SAMPLE, FISSION CROSS SECTION FOR DEPOSIT AT AVERAGE NEUTRON
C     ENERGY AND AVERAGE ACTIVATION CROSS SECTION FROM TRIAL INPUT
C
      ENAV=SUMEN1/SUMD1
      CALL INTRPL(NSIGR,ESIGR,SIGR,ENAV,SIGRAV,INDEX)
      IF(INDEX.EQ.0) GO TO 10
      ENFAV=SMEN1F/SUMD1F
      CALL INTRPL(N238,E238,SIG238,ENFAV,V238AV,INDEX)
      IF(INDEX.EQ.0) GO TO 10
C
C     NORMALIZE PROFILES
C
      PFMAX=0.0
      PSMAX=0.0
      DO 104 IP=1,NP
      IF(PF(IP).GT.PFMAX) PFMAX=PF(IP)
  104 IF(PS(IP).GT.PSMAX) PSMAX=PS(IP)
      DO 105 IP=1,NP
      PF(IP)=PF(IP)/PFMAX
  105 PS(IP)=PS(IP)/PSMAX
      SUMTOT=0.0
      DO 106 IRS=1,NRS
      DO 106 IHS=1,NHS
  106 SUMTOT=SUMTOT+YSUMS(IRS,IHS)
      DO 107 IRS=1,NRS
      VOLS=PI*RS*RS*HS*FLOAT(2*IRS-1)/FLOAT(NRS*NRS*NHS)
      DO 107 IHS=1,NHS
  107 YSUMS(IRS,IHS)=YSUMS(IRS,IHS)/SUMTOT/VOLS
C
```

```
C       COMPUTE MEASURED ACTIVATION CROSS SECTION AND CORRECTED CROSS
C       SECTION CORRESPONDING TO AVERAGE ENERGY
C
        FACTF=VMF*SUMF/RF/FLOAT(NRF)
        FACTS=VMS*ATS*SUMSP/RS/FLOAT(NRS*NHS)
        SRMEAS=YS*FACTF/YF/FACTS
        FACTK=SIGRAV*SUMD1/SUMK
        SRCEAV=FACTK*SRMEAS
C
C       PRINT VARIABLE PARAMETERS AND FINAL RESULTS
C
        IF(IWR.EQ.9) CALL AVPRT
        IF(IWR.NE.9) WRITE(IWR,200)
  200 FORMAT(//)
        WRITE(IWR,201)
  201 FORMAT(14HNT,NRF,NRS,NHS)
        WRITE(IWR,21) NT,NRF,NRS,NHS
        WRITE(IWR,202)
  202 FORMAT(17HRF,DF,RS,HS,DN,XB)
        WRITE(IWR,3000) RF,DF,RS,HS,DN,XB
 3000 FORMAT(7E11.4)
        WRITE(IWR,203)
  203 FORMAT(6HATU238)
        WRITE(IWR,3000) ATU238
        WRITE(IWR,205)
  205 FORMAT(/5H-----)
        WRITE(IWR,211)
  211 FORMAT(/)
        WRITE(IWR,31) (LABEL(I),I=1,40)
        WRITE(IWR,212)
  212 FORMAT(//22HEDIN,YF,VMF,YS,VMS,ATS)
        WRITE(IWR,3000) EDIN,YF,VMF,YS,VMS,ATS
        WRITE(IWR,213)
  213 FORMAT(31HENAV,DEMAXS,SRMEAS,FACTK,SRCEAV)
        WRITE(IWR,3000) ENAV,DEMAXS,SRMEAS,FACTK,SRCEAV
        WRITE(IWR,214)
  214 FORMAT(19HENFAV,DEMAXF,V238AV)
        WRITE(IWR,3000) ENFAV,DEMAXF,V238AV
        EFTEST=0.5*DEMAXF/FLOAT(NP)
        ESTEST=0.5*DEMAXS/FLOAT(NP)
        WRITE(IWR,215)
  215 FORMAT(4X,3HENF,1X,21H.....,4X,2HPF,  9X,3HENS,1X,2
     11H.....,4X,2HPS)
        DO 218 IP=1,NP
        VENF=EN1MF+EPF(IP)
        EFC=ABS(VENF-ENFAV)
        VENS=EN1MIN+EPS(IP)
        ESC=ABS(VENS-ENAV)
        DO 216 L=1,21
        KIF(L)=IBLANK
        IF(EFC.LT.EFTEST) KIF(L)=IDASH
        KIS(L)=IBLANK
  216 IF(ESC.LT.ESTEST) KIS(L)=IDASH
        CALL ROUND(PF(IP),INDXF)
        KIF(INDXF)=ISTAR
        CALL ROUND(PS(IP),INDXS)
        KIS(INDXS)=ISTAR
        WRITE(IWR,217)VENF,(KIF(L),L=1,21),PF(IP),VENS,(KIS(L),L=1,21),PS(
     1IP)
  217 FORMAT(F7.3,1X,21A1,1X,F5.2,5X,F7.3,1X,21A1,1X,F5.2)
  218 CONTINUE
        WRITE(IWR,219)
```

```
  219 FORMAT( 8X,21H.....,19X,21H.....)
C
C     PUNCH OUT SAMPLE ACTIVATION PROFILE ON UNIT IPN IF IPN.NE.0
C
      IF(IPN.EQ.0) GO TO 1
      WRITE(IPN,31) (LABEL(I),I=1,40)
      WRITE(IPN,21) NRS,NHS
      WRITE(IPN,22) ((YSUMS(IRS,IHS),IRS=1,NRS),IHS=1,NHS)
C
      GO TO 1
      END
      SUBROUTINE KINAM(A1,A2,A3,Q,E1,TH3,E31,E32)
C
      W1=931.478*A1
      W2=931.478*A2
      W3=931.478*A3
      W4=W1+W2-W3-Q
      EF=-Q*(1.0+(W1/W2)-(0.5*Q/W2))
      EB=-Q*(1.0+(W1/(W2-W3))-(0.5*Q/(W2-W3)))
      IF(E1-EF) 1,1,2
    1 E31=0.0
   11 E32=0.0
      GO TO 6
    2 C=COS(TH3)
      A=2.0*(W3+W4+E1+Q)
      B=2.0*E1*(W1-W4-Q)-(2.0*W4*Q+Q*Q)
      D=E1*(E1+2.0*W1)*C*C
      TERM=(B*B-2.0*W3*A*B+4.0*W3*W3*D)*E1*(E1+2.0*W1)
      IF(TERM) 1,1,3
    3 DEN=A*A-4.0*D
      U=(4.0*W3*D-A*B)/DEN
      V=2.0*C*SQRT(ABS(TERM))/DEN
      E31=U+V
      IF(E1-EB) 4,4,5
    4 IF(TH3-1.57080) 41,11,11
   41 E32=U-V
      GO TO 6
    5 E32=E31
    6 RETURN
      END
      SUBROUTINE INTRPL(N,XT,YT,X,Y,INDEX)
      DIMENSION XT(2),YT(2)
      INDEX=1
      IF(X-XT(1)) 1,3,4
    1 WRITE(4,2)
    2 FORMAT(8HRANG ERR)
      INDEX=0
      GO TO 24
    3 Y=YT(1)
      GO TO 24
    4 IF(X-XT(N)) 7,5,1
    5 Y=YT(N)
      GO TO 24
    7 I=0
      J=N
    8 K=0.5*FLOAT(J-I)+0.1
      K=K+I
      IF(X-XT(K)) 9,10,11
    9 J=K
      GO TO 12
   10 Y=YT(K)
      GO TO 24
```

```
11 I=K
12 IF(J-I-1) 13,13,8
13 I=J
   J=I-1
   DEN=XT(J)-XT(I)
   C1=(XT(J)*YT(I)-XT(I)*YT(J))/DEN
   C2=(YT(J)-YT(I))/DEN
   Y=C1+C2*X
24 RETURN
   END
   FUNCTION EXF(Z)
   IF(Z) 1,1,3
 1 IF(Z.LT.-70.0) Z=-70.0
   IF(Z.GT.-.1E-04) GO TO 2
   EXF=EXP(Z)
   GO TO 4
 3 IF(Z.GT.70.0) Z=70.0
   IF(Z.LT..1E-04) GO TO 2
   EXF=EXP(Z)
   GO TO 4
 2 EXF=1.0+Z
 4 CONTINUE
   RETURN
   END
   SUBROUTINE FINDI(N,XT,X,IX,INDEX)
   DIMENSION XT(2)
   INDEX=1
   IF(X-XT(1))1,3,4
 1 WRITE(4,2)
 2 FORMAT(8HRANG ERR)
   INDEX=0
   GO TO 24
 3 IX=1
   GO TO 24
 4 IF(X-XT(N))7,5,1
 5 IX=N-1
 7 I=0
   J=N
 8 K=0.5*FLOAT(J-I)+0.1
   K=K+I
   IF(X-XT(K))9,10,11
 9 J=K
   GO TO 12
10 IX=K-1
   GO TO 24
11 I=K
12 IF(J-I-1)13,13,8
13 IX=I
24 RETURN
   END
   SUBROUTINE SELECI(Y,N,Z,IZ)
   DIMENSION Y(2)
   NMIN=1
   NMAX=N
36 INTER=0.5*FLOAT(NMAX-NMIN)+0.1
   NTEST=NMIN+INTER
   IF(Z-Y(NTEST))1,2,3
 1 NMAX=NTEST
   GO TO 4
 2 IZ=NTEST
   GO TO 999
 3 NMIN=NTEST
```

```
    4 IF(NMAX-NMIN-1)5,5,36
    5 IZ=NMAX-1
      IF(ABS(Y(IZ+1)-Z).LT.ABS(Y(IZ)-Z)) IZ=IZ+1
  999 RETURN
      END
      SUBROUTINE ROUND(V,I)
      V20=19.99999*V
      I20=V20
      VTEST=FLOAT(I20)+0.5
      IF(V20-VTEST) 1,1,2
    1 I=I20+1
      GO TO 3
    2 I=I20+2
    3 CONTINUE
      RETURN
      END
 MON
*EOF
*REW,17
*LGO,17
```

```
2
   97
 0.0        0.0        0.449      0.0        0.45       2.865E-04  0.46       2.924E-04
 0.47       3.054E-04  0.5        3.785E-04  0.55       6.330E-04  0.58       6.946E-04
 0.59       7.630E-04  0.6        8.271E-04  0.62       9.328E-04  0.64       1.134E-03
 0.65       1.246E-03  0.66       1.301E-03  0.68       1.583E-03  0.7        1.726E-03
 0.75       2.588E-03  0.78       3.598E-03  0.8        4.495E-03  0.85       7.208E-03
 0.88       1.083E-02  0.9        1.370E-02  0.92       1.558E-02  0.95       1.663E-02
 0.97       1.591E-02  1.0        1.712E-02  1.02       1.665E-02  1.03       1.702E-02
 1.05       1.955E-02  1.08       2.480E-02  1.1        2.885E-02  1.13       3.389E-02
 1.14       3.546E-02  1.15       3.763E-02  1.17       4.047E-02  1.2        4.232E-02
 1.23       4.158E-02  1.24       4.297E-02  1.25       4.581E-02  1.28       5.916E-02
 1.3        7.059E-02  1.35       1.125E-01  1.4        1.889E-01  1.45       2.838E-01
 1.48       0.3299     1.5        0.3467     1.55       0.3802     1.6        0.4063
 1.7        0.4474     1.8        0.4891     1.9        0.5189     2.0        0.5337
 2.1        0.5388     2.2        0.5417     2.25       0.54128     2.3       0.54085
 2.309      0.54077    2.4        0.54       2.5        0.539      2.502      0.53895
 2.6        0.5364     2.7        0.5338     2.75       0.5325     2.8        0.5312
 3.0        0.5226     3.1        0.5228     3.5        0.5327     3.7        0.5439
 4.0        0.5457     4.2        0.5478     4.5        0.5492     5.0        0.5334
 5.5        0.5474     6.0        0.6126     6.2        0.6864     6.4        0.7736
 6.5        0.8091     6.6        0.8398     6.8        0.8935     7.0        0.9218
 7.5        0.9871     8.0        0.991      9.0        0.9984     10.0       0.982
 11.0       0.9867     11.5       0.9873     12.0       0.9848     13.0       1.02
 13.5       1.067      14.0       1.12       14.5       1.172      15.0       1.216
 16.0       1.272      17.0       1.274      18.0       1.288      19.0       1.336
 20.0       1.418
   23
 .0000E 00 .1268E 00 .1000E-05 .4849E-01 .1000E-01 .4826E-01 .1000E 00 .4274E-01
 .2000E 00 .7813E-01 .2500E 00 .4826E 00 .3000E 00 .1241E 00 .4000E 00 .5607E-01
 .5000E 00 .4826E-01 .6000E 00 .4780E-01 .1000E 01 .7124E-01 .1300E 01 .8043E-01
 .2000E 01 .8043E-01 .2500E 01 .8870E-01 .3000E 01 .9422E-01 .3500E 01 .9835E-01
 .4500E 01 .1172E 00 .5500E 01 .9652E-01 .6000E 01 .9881E-01 .7000E 01 .8962E-01
 .8000E 01 .8457E-01 .1500E 02 .6434E-0120.0       0.0386
   24
0.0        0.5794     0.1        0.5794     0.2        0.6881     0.318      0.427
0.428      0.602      0.514      0.5438     0.626      0.4077     0.749      0.5634
0.874      0.515      1.008      0.447      1.123      0.3564     1.248      0.4789
1.349      0.4816     1.46       0.4665     2.01       0.4402     2.5        0.4988
3.0        0.4588     4.0        0.4519     5.0        0.4437     6.04       0.4389
7.05       0.4118     8.05       0.394      14.5       0.3203     20.0       0.25
   72
0. 1000E-150. 1000E-090. 1000E+010. 1000E-090. 2821E+010. 1000E-090. 2821E+010. 1000E-09
0. 2900E+010. 7613E-040. 3000E+010. 2961E-030. 3100E+010. 6213E-030. 3200E+010. 1022E-02
0. 3300E+010. 1533E-020. 3400E+010. 2091E-020. 3500E+010. 2221E-020. 3600E+010. 2247E-02
0. 3700E+010. 3724E-020. 3800E+010. 8891E-020. 3900E+010. 1759E-010. 4000E+010. 2768E-01
0. 4100E+010. 3856E-010. 4200E+010. 4900E-010. 4300E+010. 5845E-010. 4400E+010. 6780E-01
0. 4500E+010. 7719E-010. 4600E+010. 8624E-010. 4700E+010. 9295E-010. 4800E+010. 9824E-01
0. 4900E+010. 1034E+000. 5000E+010. 1086E+000. 5100E+010. 1223E+000. 5200E+010. 1441E+00
0. 5300E+010. 1711E+000. 5400E+010. 2057E+000. 5500E+010. 2653E+000. 5600E+010. 3196E+00
0. 5700E+010. 3399E+000. 5800E+010. 3504E+000. 5900E+010. 3575E+000. 6000E+010. 3624E+00
0. 6250E+010. 3675E+000. 6500E+010. 3710E+000. 6750E+010. 3724E+000. 7000E+010. 3735E+00
0. 7250E+010. 3746E+000. 7500E+010. 3756E+000. 7750E+010. 3757E+000. 8000E+010. 3748E+00
0. 8250E+010. 3733E+000. 8500E+010. 3717E+000. 8750E+010. 3699E+000. 9000E+010. 3681E+00
0. 9250E+010. 3661E+000. 9500E+010. 3640E+000. 9750E+010. 3616E+000. 1000E+020. 3593E+00
0. 1050E+020. 3546E+000. 1100E+020. 3498E+000. 1150E+020. 3442E+000. 1200E+020. 3372E+00
0. 1250E+020. 3290E+000. 1300E+020. 3208E+000. 1350E+020. 3125E+000. 1400E+020. 3042E+00
0. 1450E+020. 2960E+000. 1500E+020. 2879E+000. 1550E+020. 2798E+000. 1600E+020. 2717E+00
0. 1650E+020. 2636E+000. 1700E+020. 2556E+000. 1750E+020. 2479E+000. 1800E+020. 2408E+00
0. 1850E+020. 2342E+000. 1900E+020. 2279E+000. 1950E+020. 2218E+000. 2000E+020. 2159E+00
   18
```

```
0.0       0.02      0.03      0.04      0.05      0.06      0.07      0.08
0.09      0.1       0.15      0.2       0.25      0.3       0.35      0.4
0.45      0.5
   19
0.0       0.087266  0.17453   0.26180   0.34907   0.43633   0.52360   0.61087
0.69813   0.78540   0.87266   0.95993   1.0472    1.1345    1.2217    1.3090
1.3963    1.4835    1.5708
0.0       4.39      20.1      54.5      109.0     181.0     260.0     328.0
384.0     413.0     336.0     212.0     143.0     103.0     84.6      69.7
58.5      50.5
0.0       4.39      20.1      54.5      109.0     181.0     260.0     328.0
383.0     413.0     335.0     212.0     143.0     103.0     84.6      69.7
58.5      50.5
0.0       4.39      20.1      54.5      109.0     181.0     260.0     328.0
383.0     412.0     335.0     212.0     143.0     103.0     84.5      69.6
58.4      50.4
0.0       4.39      20.1      54.4      109.0     181.0     259.0     328.0
383.0     412.0     335.0     212.0     142.0     103.0     84.3      69.5
58.3      50.3
0.0       4.38      20.0      54.4      109.0     181.0     259.0     327.0
382.0     412.0     334.0     211.0     142.0     102.0     84.1      69.3
58.2      50.3
0.0       4.38      20.0      54.3      109.0     180.0     259.0     327.0
382.0     411.0     334.0     211.0     142.0     102.0     83.9      69.1
58.1      50.1
0.0       4.38      20.0      54.3      109.0     180.0     258.0     326.0
381.0     410.0     333.0     210.0     141.0     102.0     83.6      68.9
57.9      50.0
0.0       4.37      20.0      54.2      108.0     180.0     258.0     326.0
380.0     409.0     332.0     210.0     141.0     101.0     83.2      68.6
57.6      49.8
0.0       4.37      19.9      54.1      108.0     180.0     257.0     325.0
379.0     408.0     331.0     209.0     140.0     101.0     82.9      68.3
57.4      49.6
0.0       4.36      19.9      54.0      108.0     179.0     257.0     324.0
378.0     407.0     330.0     208.0     140.0     100.0     82.4      67.9
57.1      49.3
0.0       4.35      19.9      53.9      108.0     179.0     256.0     323.0
377.0     406.0     329.0     207.0     139.0     100.0     82.0      67.5
56.7      49.0
0.0       4.35      19.8      53.8      108.0     178.0     255.0     322.0
376.0     404.0     327.0     206.0     138.0     99.7      81.4      67.0
56.4      48.7
0.0       4.34      19.8      53.7      107.0     178.0     255.0     321.0
375.0     403.0     326.0     205.0     138.0     99.1      80.9      66.6
56.0      48.4
0.0       4.33      19.8      53.5      107.0     177.0     254.0     320.0
374.0     401.0     324.0     204.0     137.0     98.5      80.4      66.1
55.5      48.0
0.0       4.33      19.7      53.4      107.0     177.0     253.0     319.0
372.0     400.0     323.0     203.0     136.0     97.8      79.8      65.6
55.1      47.5
0.0       4.32      19.7      53.3      106.0     176.0     252.0     318.0
371.0     398.0     321.0     202.0     135.0     97.1      79.2      65.0
54.6      47.1
0.0       4.31      19.6      53.1      106.0     176.0     251.0     317.0
369.0     397.0     320.0     201.0     134.0     96.5      78.6      64.5
54.1      46.6
0.0       4.30      19.6      53.0      106.0     175.0     250.0     316.0
368.0     395.0     318.0     200.0     133.0     95.8      78.0      63.9
53.6      46.1
0.0       4.29      19.5      52.8      105.0     174.0     249.0     314.0
```

```
366.0       393.0       316.0       198.0       132.0       95.1        77.4        63.4
53.0        45.6
   16
0.0         2.0         0.002       4.86        0.004       6.88        0.006       8.42
0.008       9.72        0.012       11.9        0.016       13.8        0.02        15.4
0.04        20.7        0.06        24.2        0.08        26.7        0.12        29.7
0.16        30.8        0.2         30.8        0.4         25.7        0.6         21.2
LI7-7
   50    50    50    10    30
1.27        0.0508      5.282       +.4988E+19+.2888E+071.1177
0.9592      0.6101      4.570       +.8079E+23+.1414E+111.1075
0.150
1
```

```
NT, NRF, NRS, NHS
   50    50    50    10
RF, DF, RS, HS, DN, XB
 0.1270E+01 0.5282E+01 0.9592E+00 0.6101E+00 0.4570E+01 0.5080E-01
ATU238
 0.4988E+19

-----


LI7-7


EDIN, YF, VMF, YS, VMS, ATS
 0.1500E+00 0.2888E+07 0.1118E+01 0.1414E+11 0.1108E+01 0.8079E+23
ENAV, DFMAXS, SRMEAS, FACTK, SRCEAV
 0.147 4E+02 0.8447E+00 0.2987E+00 0.1000E+01 0.2987E+00
ENFAV, DEMAXF, V238AV
 0.1474E+02 0.8451E+00 0.1193E+01
```

ENF		PF	ENS		PS
14.124	*	.00	14.124	*	.00
14.152	*	.00	14.153	*	.00
14.180	*	.00	14.181	*	.00
14.208	*	.00	14.209	*	.00
14.237	*	.01	14.237	*	.01
14.265	*	.01	14.265	*	.01
14.293	*	.01	14.293	*	.01
14.321	*	.01	14.321	*	.01
14.349	*	.02	14.350	*	.01
14.378	*	.03	14.378	*	.04
14.406	*	.03	14.406	*	.03
14.434	*	.09	14.434	*	.09
14.462	*	.09	14.462	*	.08
14.490	*	.15	14.490	*	.18
14.518	*	.23	14.519	*	.22
14.547	*	.30	14.547	*	.28
14.575	*	.39	14.575	*	.38
14.603	*	.50	14.603	*	.50
14.631	*	.60	14.631	*	.61
14.659	*	.70	14.659	*	.72
14.687	*	.85	14.688	*	.81
14.716	*	.90	14.716	*	.92
14.744	*-	.95	14.744	*-	.96
14.772	*	1.00	14.772	*	1.00
14.800	*	.94	14.800	*	.95
14.828	*	.94	14.828	*	.98
14.856	*	.90	14.856	*	.89
14.885	*	.92	14.885	*	.92
14.913	*	.83	14.913	*	.92
14.941	*	.11	14.941	*	.17

```
LI7-7
   50    10
0.6584E+000.6584E+000.6583E+000.6582E+000.6581E+000.6579E+000.6578E+000.6576E+00
0.6574E+000.6571E+000.6569E+000.6566E+000.6563E+000.6560E+000.6557E+000.6553E+00
0.6549E+000.6545E+000.6541E+000.6536E+000.6531E+000.6527E+000.6521E+000.6516E+00
0.6511E+000.6505E+000.6499E+000.6493E+000.6486E+000.6480E+000.6473E+000.6466E+00
0.6459E+000.6451E+000.6444E+000.6436E+000.6428E+000.6420E+000.6411E+000.6403E+00
0.6394E+000.6385E+000.6376E+000.6367E+000.6358E+000.6348E+000.6338E+000.6328E+00
0.6318E+000.6308E+000.6388E+000.6387E+000.6386E+000.6386E+000.6384E+000.6383E+00
0.6381E+000.6380E+000.6378E+000.6376E+000.6373E+000.6370E+000.6368E+000.6365E+00
```

0.6361E+000.6358E+000.6354E+000.6350E+000.6346E+000.6342E+000.6338E+000.6333E+00
0.6328E+000.6323E+000.6318E+000.6312E+000.6307E+000.6301E+000.6295E+000.6288E+00
0.6282E+000.6275E+000.6269E+000.6262E+000.6254E+000.6247E+000.6239E+000.6232E+00
0.6224E+000.6216E+000.6207E+000.6199E+000.6190E+000.6181E+000.6173E+000.6164E+00
0.6154E+000.6145E+000.6135E+000.6126E+000.6199E+000.6199E+000.6198E+000.6197E+00
0.6196E+000.6195E+000.6193E+000.6191E+000.6190E+000.6187E+000.6185E+000.6183E+00
0.6180E+000.6177E+000.6174E+000.6171E+000.6167E+000.6164E+000.6160E+000.6156E+00
0.6151E+000.6147E+000.6142E+000.6138E+000.6133E+000.6127E+000.6122E+000.6117E+00
0.6111E+000.6105E+000.6099E+000.6093E+000.6086E+000.6079E+000.6073E+000.6066E+00
0.6058E+000.6051E+000.6044E+000.6036E+000.6028E+000.6020E+000.6012E+000.6003E+00
0.5995E+000.5986E+000.5978E+000.5969E+000.5960E+000.5950E+000.6018E+000.6018E+00
0.6017E+000.6016E+000.6015E+000.6014E+000.6012E+000.6011E+000.6009E+000.6007E+00
0.6005E+000.6002E+000.6000E+000.5997E+000.5994E+000.5991E+000.5988E+000.5984E+00
0.5981E+000.5977E+000.5973E+000.5969E+000.5964E+000.5960E+000.5955E+000.5950E+00
0.5945E+000.5940E+000.5934E+000.5929E+000.5923E+000.5917E+000.5911E+000.5904E+00
0.5898E+000.5891E+000.5884E+000.5877E+000.5870E+000.5863E+000.5856E+000.5848E+00
0.5840E+000.5832E+000.5824E+000.5816E+000.5808E+000.5799E+000.5791E+000.5782E+00
0.5844E+000.5844E+000.5843E+000.5842E+000.5841E+000.5840E+000.5839E+000.5837E+00
0.5836E+000.5834E+000.5832E+000.5829E+000.5827E+000.5824E+000.5822E+000.5819E+00
0.5816E+000.5812E+000.5809E+000.5805E+000.5801E+000.5797E+000.5793E+000.5789E+00
0.5784E+000.5780E+000.5775E+000.5770E+000.5765E+000.5759E+000.5754E+000.5748E+00
0.5742E+000.5736E+000.5730E+000.5724E+000.5717E+000.5711E+000.5704E+000.5697E+00
0.5690E+000.5683E+000.5675E+000.5668E+000.5660E+000.5652E+000.5644E+000.5636E+00
0.5628E+000.5620E+000.5677E+000.5677E+000.5676E+000.5675E+000.5674E+000.5673E+00
0.5672E+000.5671E+000.5669E+000.5667E+000.5665E+000.5663E+000.5661E+000.5658E+00
0.5656E+000.5653E+000.5650E+000.5647E+000.5643E+000.5640E+000.5636E+000.5632E+00
0.5629E+000.5624E+000.5620E+000.5616E+000.5611E+000.5606E+000.5601E+000.5596E+00
0.5591E+000.5586E+000.5580E+000.5575E+000.5569E+000.5563E+000.5557E+000.5550E+00
0.5544E+000.5537E+000.5530E+000.5523E+000.5516E+000.5509E+000.5502E+000.5494E+00
0.5487E+000.5479E+000.5471E+000.5464E+000.5517E+000.5516E+000.5516E+000.5515E+00
0.5514E+000.5513E+000.5512E+000.5510E+000.5509E+000.5507E+000.5505E+000.5503E+00
0.5501E+000.5499E+000.5496E+000.5493E+000.5491E+000.5488E+000.5484E+000.5481E+00
0.5478E+000.5474E+000.5470E+000.5466E+000.5462E+000.5458E+000.5454E+000.5449E+00
0.5445E+000.5440E+000.5435E+000.5430E+000.5424E+000.5419E+000.5413E+000.5408E+00
0.5402E+000.5396E+000.5390E+000.5383E+000.5377E+000.5370E+000.5364E+000.5357E+00
0.5350E+000.5343E+000.5336E+000.5328E+000.5321E+000.5313E+000.5362E+000.5362E+00
0.5361E+000.5361E+000.5360E+000.5359E+000.5358E+000.5356E+000.5355E+000.5353E+00
0.5351E+000.5349E+000.5347E+000.5345E+000.5343E+000.5340E+000.5337E+000.5335E+00
0.5332E+000.5328E+000.5325E+000.5322E+000.5318E+000.5314E+000.5311E+000.5307E+00
0.5302E+000.5298E+000.5294E+000.5289E+000.5284E+000.5279E+000.5274E+000.5269E+00
0.5264E+000.5259E+000.5253E+000.5247E+000.5241E+000.5235E+000.5229E+000.5223E+00
0.5217E+000.5210E+000.5204E+000.5197E+000.5190E+000.5183E+000.5176E+000.5169E+00
0.5214E+000.5213E+000.5213E+000.5212E+000.5211E+000.5210E+000.5209E+000.5208E+00
0.5207E+000.5205E+000.5203E+000.5201E+000.5199E+000.5197E+000.5195E+000.5193E+00
0.5190E+000.5187E+000.5185E+000.5182E+000.5178E+000.5175E+000.5172E+000.5168E+00
0.5164E+000.5161E+000.5157E+000.5153E+000.5148E+000.5144E+000.5140E+000.5135E+00
0.5130E+000.5125E+000.5120E+000.5115E+000.5110E+000.5104E+000.5099E+000.5093E+00
0.5087E+000.5081E+000.5075E+000.5069E+000.5063E+000.5056E+000.5050E+000.5043E+00
0.5036E+000.5029E+000.5071E+000.5070E+000.5070E+000.5069E+000.5068E+000.5067E+00
0.5066E+000.5065E+000.5064E+000.5062E+000.5061E+000.5059E+000.5057E+000.5055E+00
0.5053E+000.5051E+000.5048E+000.5046E+000.5043E+000.5040E+000.5037E+000.5034E+00
0.5031E+000.5027E+000.5024E+000.5020E+000.5016E+000.5013E+000.5009E+000.5004E+00
0.5000E+000.4996E+000.4991E+000.4986E+000.4982E+000.4977E+000.4972E+000.4966E+00
0.4961E+000.4956E+000.4950E+000.4944E+000.4939E+000.4933E+000.4927E+000.4921E+00
0.4914E+000.4908E+000.4901E+000.4895E+00

Note: IPN=9 prints activity profile along with the rest of the output.

```
NT, NRF, NRS, NHS
   50    50    50    10
RF, DF, RS, HS, DN, XB
 0.1270E+01 0.5282E+01 0.9592E+00 0.6101E+00 0.4570E+01 0.5080E-01
ATU238
 0.4988E+19

-----

LI7-7

EDIN, YF, VMF, YS, VMS, ATS
 0.1500E+00 0.2888E+07 0.1118E+01 0.1414E+11 0.1108E+01 0.8079E+23
ENAV, DEMAXS, SRMEAS, FACTK, SRCEAV
 0.1474E+02 0.8447E+00 0.2987E+00 0.1000E+01 0.2987E+00
ENFAV, DEMAXF, V238AV
 0.1474E+02 0.8451E+00 0.1193E+01
```

ENF	PF	ENS	PS
14.124	.00	14.124	.00
14.152	.00	14.153	.00
14.180	.00	14.181	.00
14.208	.00	14.209	.00
14.237	.01	14.237	.01
14.265	.01	14.265	.01
14.293	.01	14.293	.01
14.321	.01	14.321	.01
14.349	.02	14.350	.01
14.378	.03	14.378	.04
14.406	.03	14.406	.03
14.434	.09	14.434	.09
14.462	.09	14.462	.08
14.490	.16	14.490	.18
14.518	.23	14.519	.22
14.547	.30	14.547	.28
14.575	.39	14.575	.38
14.603	.50	14.603	.50
14.631	.60	14.631	.61
14.659	.70	14.659	.72
14.687	.85	14.688	.81
14.716	.90	14.716	.92
14.744	.95	14.744	.96
14.772	1.00	14.772	1.00
14.800	.94	14.800	.95
14.828	.94	14.828	.98
14.856	.90	14.856	.89
14.885	.92	14.885	.92
14.913	.83	14.913	.92
14.941	.11	14.941	.17

Note: IPN=0 suppresses activity profile output.

REFERENCES

1. Mohamed A. Abdou, "Tritium Breeding in Fusion Reactors" in Nuclear Data for Science and Technology, Proceedings of the International Conference, 6-10 September 1982, Antwerp, Belgium, Ed. K. H. Böckhoff, D. Reidel Publishing Company, Dordrecht, Holland, p. 293 (1983).

2. WRENDA 83/84, "World Request List for Nuclear Data", Ed. V. Piksaikin, INDC(SEC)-88/URSF, International Atomic Energy Agency, Vienna (1983).

3. E. T. Cheng, D. R. Mathews and K. R. Schultz, "Magnetic Fusion Energy Program Nuclear Data Needs", GA-A17324 (UC-20), GA Technologies (1983).

4. G. M. Hale, "The $^{6}Li(n,t)^{4}He$ Cross Section" in Nuclear Data Standards for Nuclear Data Measurements, Eds. H. Conde, A. B. Smith and A. Lorenz, INDC Nuclear Standards Subcommittee, Technical Report Series No. 227, International Atomic Energy Agency, Vienna, p. 11 (1983).

5. M. T. Swinhoe, "Tritium Breeding in Fusion" in Nuclear Cross Sections for Technology, Proceedings of the International Conference, October 22-26, 1979, Knoxville, Tennessee, U.S.A., Eds. J. L. Fowler, C. H. Johnson and C. D. Bowman, NBS Special Publication No. 594, U. S. Department of Commerce, Washington, D. C., p. 246 (1980).

6. R. C. Haight, "Neutron Cross Sections for Fusion", ibid. Ref. 5, p. 228.

7. "Evaluated Neutron Data File, ENDF/B-IV, National Nuclear Data Center, Brookhaven National Laboratory, Upton, N. Y. 11973, U.S.A. (1975).

8. M. Swinhoe and C. Uttley, AERE-R-9929, Harwell, U.K. (1980).

9. Donald L. Smith, Manuel M. Bretscher and James W. Meadows, Nucl. Sci. Eng. 78, 359 (1981).

10. M. M. Bretscher and D. L. Smith, "Thermal Neutron Calibration of a Tritium Extraction Facility Using the $^{6}Li(n,t)^{4}He/^{197}Au(n,\gamma)^{198}Au$ Cross Section Ratio for Standardization", ANL/NDM-55, Argonne National Laboratory (1980).

11. H. Liskien and A. Paulsen, Annals of Nuclear Energy 8, 423 (1981).

12. "Evaluated Neutron Data File, ENDF/B-V", National Nuclear Data Center, Brookhaven National Laboratory, Upton, N.Y., U.S.A. (1979).

13. P. Young, LA-8874-PR, Los Alamos National Laboratory, Los Alamos, New Mexico, U.S.A. (1981); also Trans. Am. Nucl. Soc. 39, 272 (1981) and private communication (1982 and 1984).

14. H. Liskien, R. Wölfe and S. M. Qaim, "Determination of $^{7}Li(n,n't)^{4}He$ Cross Sections", ibid. Ref. 1, p. 349.

15. S. A. Cox and P. R. Hanley, IEEE Trans. Nucl. Sci. 18, 108 (1971).

16. H. H. Barschall, "14 MeV D-T Sources" in Neutron Sources for Basic Physics and Applications, Vol. 2 in the Nuclear Energy Agency Nuclear Data Committee (OECD) series "Neutron Physics and Nuclear Data in Science and Technology", Eds. A. Michaudon, S. Cierjacks and R. E. Chrien, Pergamon Press, Oxford, p. 57 (1983).

17. Texas Nuclear Generator Model No. 9400: Texas Nuclear Corporation (a subsidiary of Nuclear Chicago Corporation), P. O. Box 9267, Austin, Texas 78756.

18. Safety Light Corporation, 4150A Old Berwick Road, Bloomsburg, Pennsylvania 17815.

19. G. Winkler and T. B. Ryves, Ann. Nucl. Energy 10, 601 (1983).

20. A. Tsechanski and G. Shani, Nucl. Sci. Eng. 87, 189 (1984).

21. Stable Isotopes Division, Oak Ridge National Laboratory, Oak Ridge, Tennessee 37830.

22. J. W. Meadows, Nucl. Sci. Eng. 49, 310 (1972).

23. Donald L. Smith and James W. Meadows, "Response of Several Threshold Reactions in Reference Fission Neutron Fields", ANL/NDM-13, Argonne National Laboratory, Argonne, Illinois 60439 (1975).

24. W. P. Poenitz, J. W. Meadows and R. J. Armani, "^{235}U Fission Mass and Counting Comparison and Standardization", ANL/NDM-48, Argonne National Laboratory, Argonne, Illinois 60439 (1979).

25. M. M. Bretscher, "Li-6 as a Reference Absorber for Capture-to-Fission Ratio Measurements in Zero Power Fast Critical Assemblies", Reactor Physics Division Annual Report, July 1, 1967 to June 30, 1968, ANL-7410, pp. 178-182, Argonne National Laboratory (1969).

26. M. M. Bretscher, B. M. Oliver and Harry Farrar IV", Calibrations of a Tritium Extraction Facility", paper presented at the 10^{th} Symposium on Fusion Engineering, Philadelphia, Pennsylvania, December 5-9, 1983. Proceedings are available in book and microfiche form from IEEE Service Center, Single Publication Sales Department, 445 Hoes Lane, Piscataway, New Jersey 08854.

27. Model 2660 Packard Tri-Carb Liquid Scintillation Counter: Packard Instrument Co., Inc., 2200 Warrenville Road, Downers Grove, Illinois 60515.

28. M. P. Unterweger, B. M. Coursey, F. J. Schima and W. B. Mann, "Preparation and Calibration of the 1978 National Bureau of Standards Tritiated Water Standards", Int. J. Appl. Rad. and Isotopes 31, 611 (1980). See also A Handbook of Radioactivity Measurements Procedures, NCRP Report No. 58, p. 322 (1978).

29. R. L. Henkel and J. E. Brolley, Jr., Phys. Rev. 103, 1292 (1956).

30. F. William Walker, George J. Kirouac and Francis M. Rourke, "Chart of the Nuclides-Twelfth Edition", Knolls Atomic Power Laboratory, General Electric Company, Schenectady, New York 12345 (1977).

31. Table of the Isotopes, 7th Edition, Eds. C. Michael Lederer and Virginia S. Shirley, John Wiley and Sons, Inc., New York (1978).

B. M. Oliver and Harry Farrar IV, Rockwell International Corporation, Energy Systems Group, 8900 Desoto Avenue, Canoga Park, California 91304 (private communication, 1983).

33. Donald L. Smith and James W. Meadows, "Measurement of $^{58}Ni(n,p)^{58}Co$ Reaction Cross Sections for E_n=0.44-5.87 MeV using Activation Methods", ANL-7989, Argonne National Laboratory, Argonne, Illinois 60439 (1973).

34. D. L. Smith and J. W. Meadows, "Neutron Inelastic Scattering Studies for Lead-204", ANL/NDM-37, Argonne National Laboratory, Argonne, Illinois 60439 (1977).

35. D. L. Smith and J. W. Meadows, "Method of Neutron Activation Cross Section Measurement for E_n=5.5-10 MeV Using the D(d,n)He-3 Reaction as a Neutron Source", ANL/NDM-9, Argonne National Laboratory, Argonne Illinois 60439 (1974).

36. Donald L. Smith, "Some Comments on Resolution and the Analysis and Interpretation of Experimental Results from Differential Neutron Measurements", ANL/NDM-49, Argonne National Laboratory, Argonne, Illinois 60439 (1979).

37. Donald L. Smith, "A Least-Squares Method for Deriving Reaction Differential Cross Section Information from Measurements Performed in Diverse Neutron Fields", ANL/NDM-77, Argonne National Laboratory, Argonne, Illinois 60439 (1982).

38. H. Liskien and A. Paulsen, "Neutron Production Cross Sections and Energies for the Reactons $T(p,n)^3He$, $D(d,n)^3He$, $T(d,n)^4He$, Nuclear Data Tables 11, 569-619 (1973).

39. H. H. Anderson and J. F. Ziegler, Hydrogen-Stopping Powers and Ranges in all Elements, Vol. 3, Pergamon Press, New York (1977).

40. A. Poularikas and D. G. Gardner, Ann. Prog. Rep. Nucl. Chem., Univ. of Arkansas (1963).

41. S. M. Qaim, R. Wölfe and G. Stöcklin, Proc. Int. Conf. on Chemical Nuclear Data: Measurement and Applications, Canterbury, U.K., p. 121 (1971).

42. S. M. Qaim and G. Stöcklin, J. Inorg. Nucl. Chem. 35, 19 (1973).

43. S. M. Qaim and G. Stöcklin, Nucl. Phys. A257, 233 (1976).

44. S. M. Qaim and R. Wölfe, Nucl. Phys. A295, 150 (1978).

45. J. W. Meadows, "The Fission Cross Sections of Some Thorium, Uranium, Neptunium and Plutonium Isotopes Relative to ^{235}U", ANL/NDM-83, Argonne National Laboratory (1983).

46. W. P. Poenitz and J. W. Meadows, "^{235}U and ^{239}Pu Sample-Mass Determinations and Intercomparisons", ANL/NDM-84, Argonne National Laboratory (1983).

47. W. Poenitz, E. Pennington, A. B. Smith and R. Howerton, "Evaluated Fast Neutron Cross Sections of Uranium-238", ANL/NDM-32, Argonne National Laboratory (1977).

48. Donald L. Smith, "Covariance Matrices and Applications to the Field of Nuclear Data", ANL/NDM-62, Argonne National Laboratory (1981).

49. M. E. Wyman and M. M. Thorpe, "A Measurement of the $^{7}Li(n,n'\alpha)t$ Cross Section for Several Neutron Energies", LA-2235, Los Alamos National Laboratory (1958).

50. A. R. Osborn and H. W. Wilson, "Production of Tritium in Li-7 by MeV Neutrons", AWRE-NR/C-1, p. 61, Atomic Weapons Research Establishment, Aldermaston, United Kingdom (1961).

51. F. Brown, R. H. James, J. L. Perkin and J. Barry, J. Nucl. Energy A/B 17, 137 (1963).

52. R. Batchelor and J. H. Towle, Nucl. Phys. 47, 385 (1963).

53. J. A. Cookson, D. Dandy and John C. Hopkins, Nucl. Phys. A91, 273 (1967).

54. J. C. Hopkins, D. M. Drake and H. Conde, Nucl. Phys. A107, 139 (1968).

55. H. D. Knox, R. M. White and R. O. Lane, Nucl. Sci. Eng. 69, 223 (1979).

56. Glen M. Frye, Jr., Phys. Rev. 93, 1086 (1954).

57. L. Rosen, "Fast Neutron Interactions with ^{6}Li and ^{7}Li", LAMS-2979, Los Alamos National Laboratory (1963).

58. L. Rosen and L. Stewart, Phys. Rev. 126, 1150 (1962).

59. R. G. Thomas, "Determination of the 14-MeV $^{7}Li(n,n't)\alpha$ Cross Section from Sphere Multiplication and Transmission Measurements", LA-1697, Los Alamos National Laboratory (1954).

Table 1: Lithium-Sample Properties

Sample	Total Mass (g)	Al Capsule Mass (g)	Lithium Mass (g)	Lithium Pellet[c] Thickness (cm)
^{7}Li#3[a]	2.7129	1.8593	0.8536	0.553
^{7}Li#7[b]	2.8093	1.8676	0.9417	0.610
^{7}Li#23[b]	2.6583	1.8442	0.8141	0.527
^{7}Li#24[b]	2.8194	1.8329	0.9865	0.639

[a]Unirradiated sample.

[b]Irradiated sample.

[c]Based on a uniform diameter of 1.918 cm and an assumed density of 0.534 gm/cm^3.

Table 2: Summary of Tritium Data for the 14-MeV $^{7}Li(n,n't)^{4}He$ Cross-Section Measurement[a]

Sample	Extract. Date	Ref. Date	m(E) H_2O-g	$\frac{m(C)}{m(E)}$	m(Li) g	dps/g H_2O	dps/g Li	1σ Random Error,%
BKG-1	8-30-83	11-12-83	5.71603	1.00038		0.1728		4.2
^{7}Li#3	8-30-83	11-12-83	5.66418	1.00669	0.85358	0.0921	0.6150	8.1
BKG-2	8-31-83	11-12-83	5.72004	1.00250		0.0508		14.7
^{7}Li#7	8-31-83	11-12-83	5.66803	1.01080	0.94166	4.3955	26.7427	1.0
BKG-3	9-1-83	11-12-83	5.75665	1.00071		-0.0054		125.2
^{7}Li#23	9-1-83	11-12-83	5.69645	1.00597	0.81411	3.3798	23.7902	0.7
BKG-4	9-2-83	11-12-83	5.7614	1.00380		-0.00813		90.2
^{7}Li#24	9-2-83	11-12-83	5.68660	1.00936	0.98651	3.8745	22.5430	0.5
BKG-5[b]	9-3-83	11-12-83	5.76572	1.00041		0.1752		4.1

[a]Activities given here are based on the NBS tritium standard [28]. Final cross section determination, however, takes into account an upward revision of this standard by 0.7%, based on work at Rockwell International Corporation [26].

[b]Same liner as BKG-1.

Table 3: Selected Cross-Section Neutron-Energy Sensitivities at 14.7 MeV[a]

Reaction	Effective[b] Threshold (MeV)	$100(d\sigma/dE)/\sigma$ ($\% \cdot MeV^{-1}$)
$^{238}U(n,f)$	1.0	8.2
$^{56}Fe(n,p)^{56}Mn$	5.0	-12.0
$^{58}Ni(n,p)^{58}Co$	0.4	-26.3
$^{58}Ni(n,2n)^{57}Ni$	12.5	42.8

[a]Based on ENDF/B-V [12].

[b]These are "effective" thresholds, designating energies where the cross sections becomes negligible when compared to the values ~ 14.7 MeV.

Table 4: Calculated Neutron Scattering Corrections

Origin	Fission Events (%)	Tritium-Production Events (%)
Target structures	7.64	7.82
^{7}Li-sample and capsule	2.51	2.73
Fission Detector	1.62	0.20
Total	11.77	10.75

Table 5: Spectral-Indicator Results (Energy Shift Interpretation)

Spectral Indicator Ratio	Percent Change in [a] Ratio per Coulomb Accumulated Charge	100 $(dR/dE)/R$[b] ($\% \cdot MeV^{-1}$)	ΔE[c] (MeV)
$^{238}U(n,f)/LC$	0.128	~ 8.2	0.080
$^{56}Fe(n,p)/LC$	0.073	~ -12.0	-0.030
$^{58}Ni(n,p)/LC$	0.435	~ -26.3	-0.080
$^{58}Ni(n,2n)/LC$	0.470	~ +42.8	0.055
$^{56}Fe(n,p)/^{238}U(n,f)$	-0.071	-19.4	0.020
$^{58}Ni(n,p)/^{238}U(n,f)$	0.262	-34.5	-0.040
$^{58}Ni(n,2n)/^{238}U(n,f)$	0.192	+34.6	0.030
$^{58}Ni(n,2n)/^{58}Ni(n,p)$	-0.129	+70.3	-0.010
Average	-	-	0.003

[a]Based on least-squares fits to measured values.

[b]Derived from ENDF/B-V[12]. A flat long-counter (LC) response is assumed where applicable.

[c]Column 4 values obtained by dividing Column 2 values by Column 3 values and multiplying the results by 5 Coulombs, the assumed typical target life.

Table 6: Spectral-Indicator Results (Deuterium Buildup Interpretation)

Spectral[a] Indicator Ratio	$[\sigma(2.5)/\sigma(14.7)-\sigma_m(2.5)/\sigma_m(14.7)]$[b]	a[c]	(aQ) for Q=5 Coulombs (in %)
$^{56}Fe(n,p)/^{238}U(n,f)$	-0.446	0.00159	0.80
$^{58}Ni(n,p)/^{238}U(n,f)$	0.786	0.00333	1.66
$^{58}Ni(n,2n)/^{238}U(n,f)$	-0.446	-0.00430	-2.15
$^{58}Ni(n,2n)/^{58}Ni(n,p)$	-0.357	0.00361	1.81
Average	-	-	0.53 ± 0.79

[a]Only reaction-ratio indicators are considered.

[b]Based on ENDF/B-V [12].

[c]Derived from least-squares fit to spectral-indicator data.

Table 7: Sources of Experimental Error

RANDOM ERRORS (%)

Source	^{7}Li#7	^{7}Li#23	^{7}Li#24
Lithium sample mass	N[a]	N	N
Water sample mass	N	N	N
Tritium-recovery losses	0.4	0.4	0.4
Tritium-counting statistics	1	0.7	0.5
Tritium-counting facility background	0.1	0.1	0.1
Contamination effects	0.2	N	N
Fission-counting statistics	0.1	0.1	0.1
Fissions extrapolation correction	N	N	N
Geometric effects	0.2	0.2	0.2
Escape of tritium from Al capsules	N	N	N
Total random error in ratio	1.1	0.8	0.7

SYSTEMATIC ERRORS (%)

Source	All Li Samples
Tritium half life	0.3
Tritiated water standard	0.6
Calibration of tritium-counting facility	0.3
Activity decay correction	N
^{7}Li isotopic abundance	N
^{6}Li(n,t)α effects	N
U-238 deposit mass	0.9
Fissions extrapolation correction	1.6
Fissions deposit-thickness correction	0.5
Neutron source representation	N
Uncorrected neutron scattering from environment	0.1
Neutron absorption	0.3
Neutron multiple scattering	0.3
Average neutron energy	0.1
Geometric effects	0.2
Computational methods	N
Al(n,X)t effects	N
Total systematic error in ratio	2.1

Error in ^{238}U(n,f) Cross-section standard: 4.8%

[a]N=negligible

Table 8: Principal Results of the Present Experiment

Neutron Spectrum

Average energy = 14.74 MeV
Uncertainty in the average energy = ± 0.02 MeV
FWHM resolution of neutron distribution = 0.324 MeV (see Fig. 5)

Ratios and Cross Sections

ENDF/B-V [12] standard ^{238}U neutron-fission cross section = 1.193[b]
Probable error in the standard cross section = 4.8% (see Section IV of text)

Individual Ratios and Cross Sections:

Sample	Measured Ratio	Ratio Random Error (%)	Derived $^{7}Li(n,n't)^{4}He$ Cross Section (b)
^{7}Li#7	0.2512	1.1	0.2997
^{7}Li#23	0.2528	0.8	0.3016
^{7}Li#24	0.2523	0.7	0.3010

Weighted average of the ratios = 0.2523
Random error in weighted average of the ratios = 0.5%
Systematic error in the ratios = 2.1%
Total error in weighted average of the ratios = 2.2%
Weighted average of the $^{7}Li(n,n't)^{4}He$ cross sections = 0.3010[b]
Total error in weighted average of the $^{7}Li(n,n't)^{4}He$ cross sections = 5.3%
(includes 4.8% error in the standard cross section).

FIGURE CAPTIONS

Figure 1: Summary of experimental data available for the $^{7}Li(n,n't)^{4}He$ reaction prior to the present experiment: Refs. 5 and 8 (O); Ref. 9 (●); Ref. 11 (▲); Ref. 14 (Δ); Ref. 49 (X); Ref. 50 (■); Ref. 51 (⧗); Ref. 52 (⊖); Ref. 53 (▣); Ref. 54 (◇); Ref. 55 (▦); Ref. 56 (▩); Refs. 57 and 58 (□); Ref. 59 (◆). Prior evaluations discussed in Section I are also shown: Ref. 7, ENDF/B-IV, and Ref. 12, ENDF/B-V original (---); Ref. 13, Young evaluation accepted as ENDF/B-V. Rev. 2 (——).

Figure 2: Schematic diagram of Ti-T target assembly and fission-detector apparatus used for irraditions in the present experiment.

Figure 3: Schematic diagram of apparatus used to extract tritium from irradiated samples.

Figure 4: Typical history for utilization of a Ti-T target in the present experiment. Abscissa indicates the integrated beam time on target while the ordinate indicates the average yields of neutrons during the indicated sample irradiations. Beam-off time is not shown.

Figure 5: Characteristic effective neutron spectrum for the present experiment, corresponding to 150-keV incident deuterons. The differences in the spectra seen by the samples and the uranium deposit were negligible.

Figure 6: Summary of experimental data and evaluations in the vicinity of 14 MeV for the $^{7}Li(n,n't)^{4}He$ reaction. Experimental values: Present work (●); Refs. 5 and 8 (O); Ref. 14 (Δ); Ref. 49 (X); Ref. 50 (▣); Ref. 51 (⧗); Ref. 56 (▩); Ref. 57 (□). Evaluations: Ref. 7, ENDF/B-IV, and Ref. 12, ENDF/B-V original (---); Ref. 13, Young evaluation accepted as ENDF/B-V. Rev. 2 (——).

Figure 7: Schematic diagram indicating major elements of the geometry for cross section calculations with code ACTV14.

Figure 1

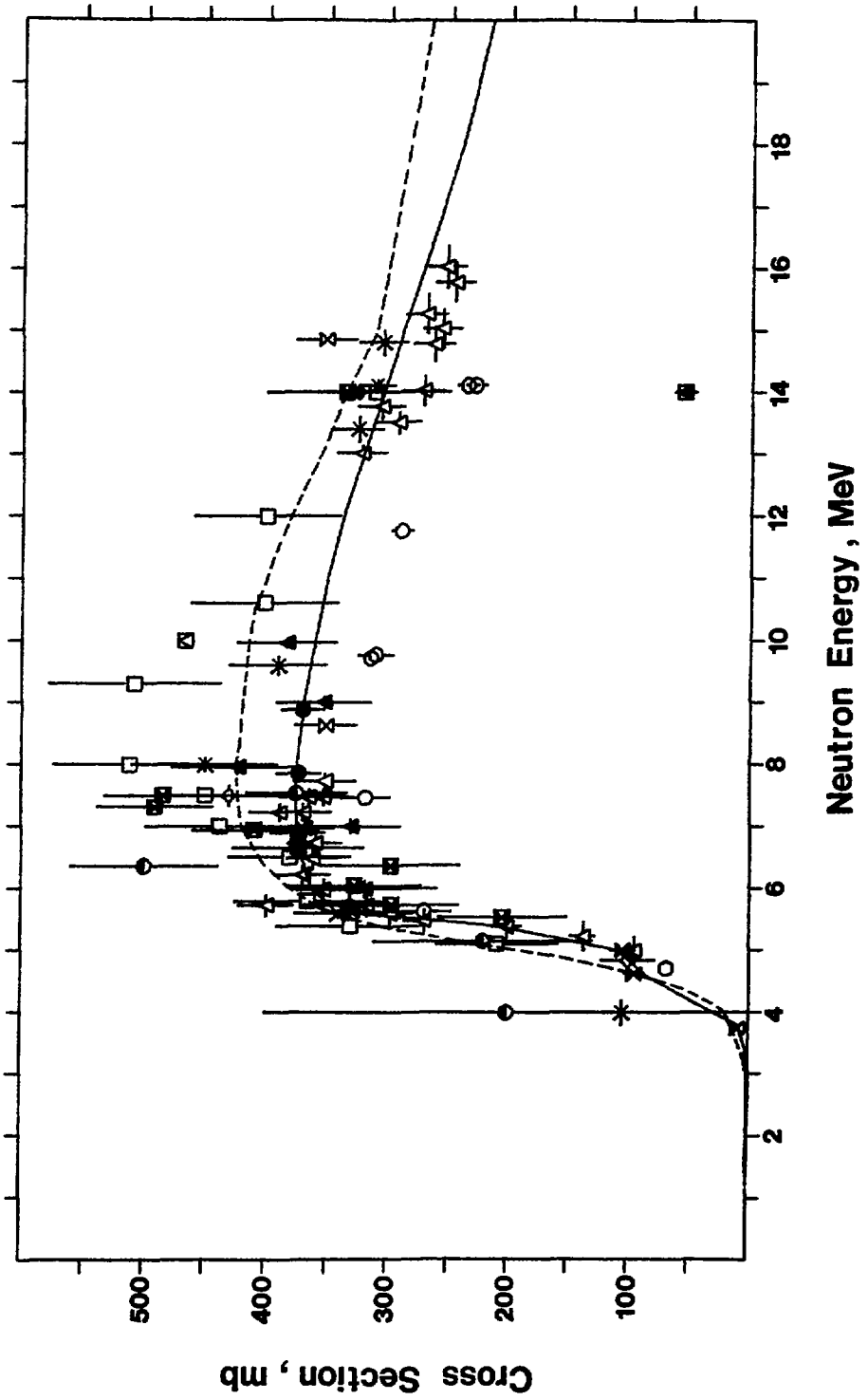
Cross Section , mb
500
400
300
200
100
Neutron Energy , MeV
2
4
6
8
10
12
14
16
18

Figure 2

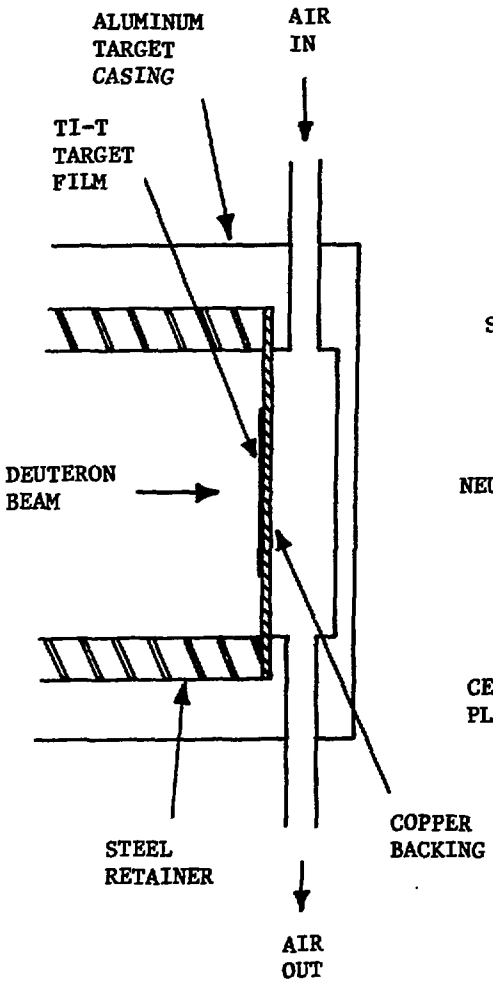

TARGET ASSEMBLY

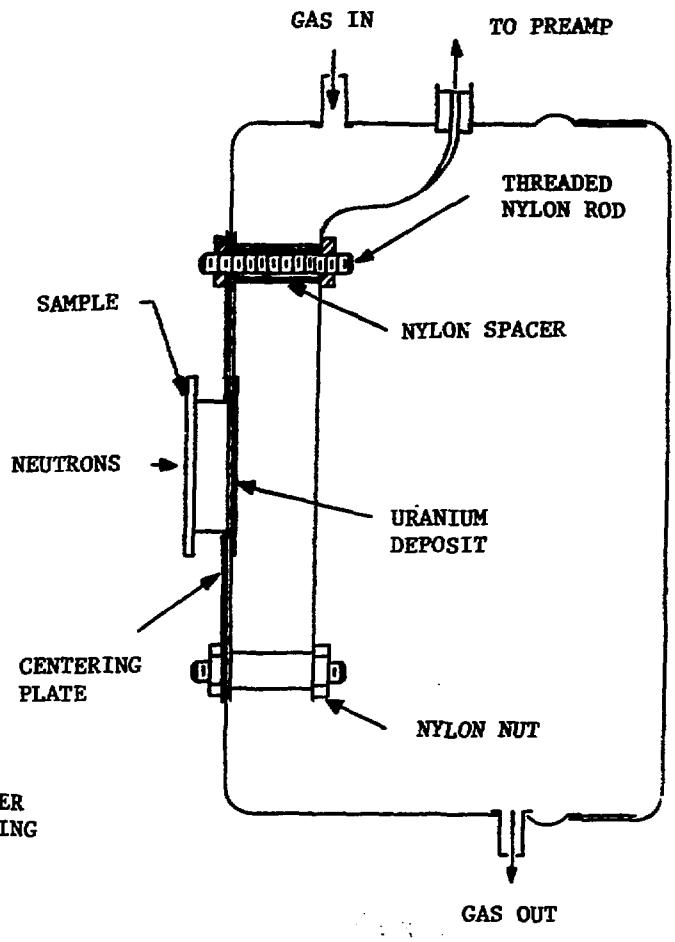

FISSION CHAMBER

TRITIUM EXTRACTION SYSTEM

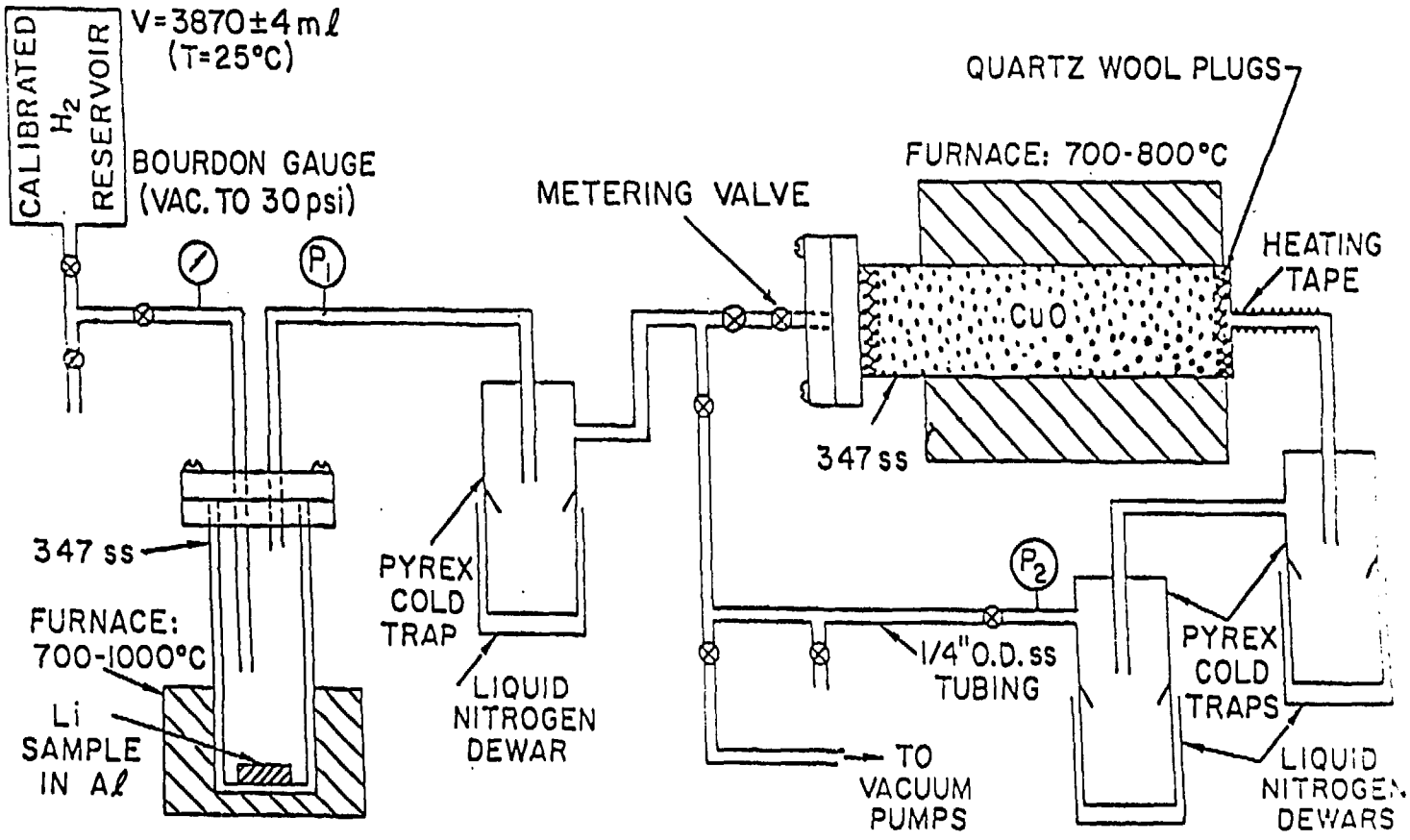

Figure 3

Figure 4

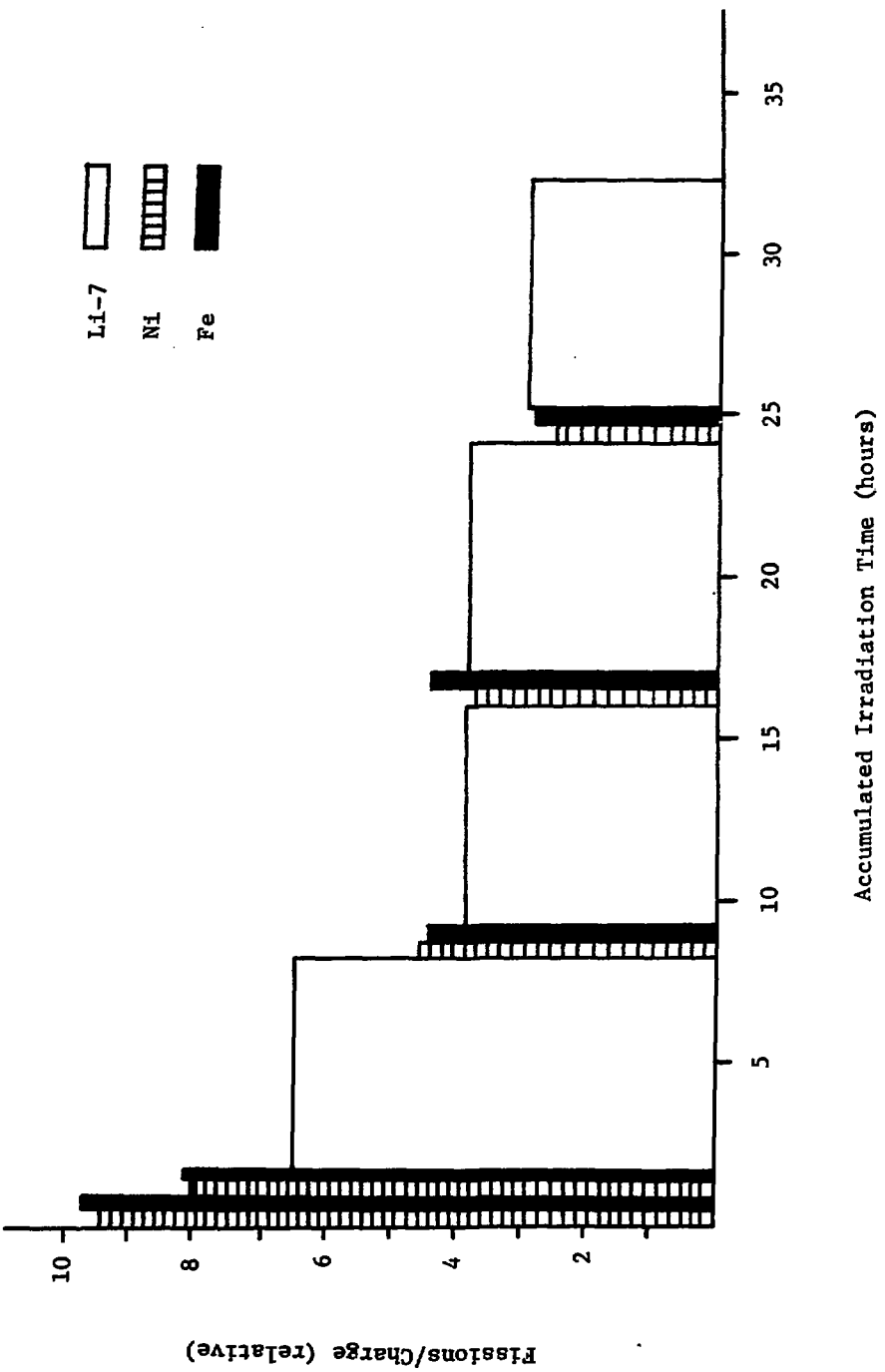
Li-7
Ni
Fe
Fissions/Charge (relative)
2
4
6
8
10
5
10
15
20
25
30
35
Accumulated Irradiation Time (hours)

Figure 5

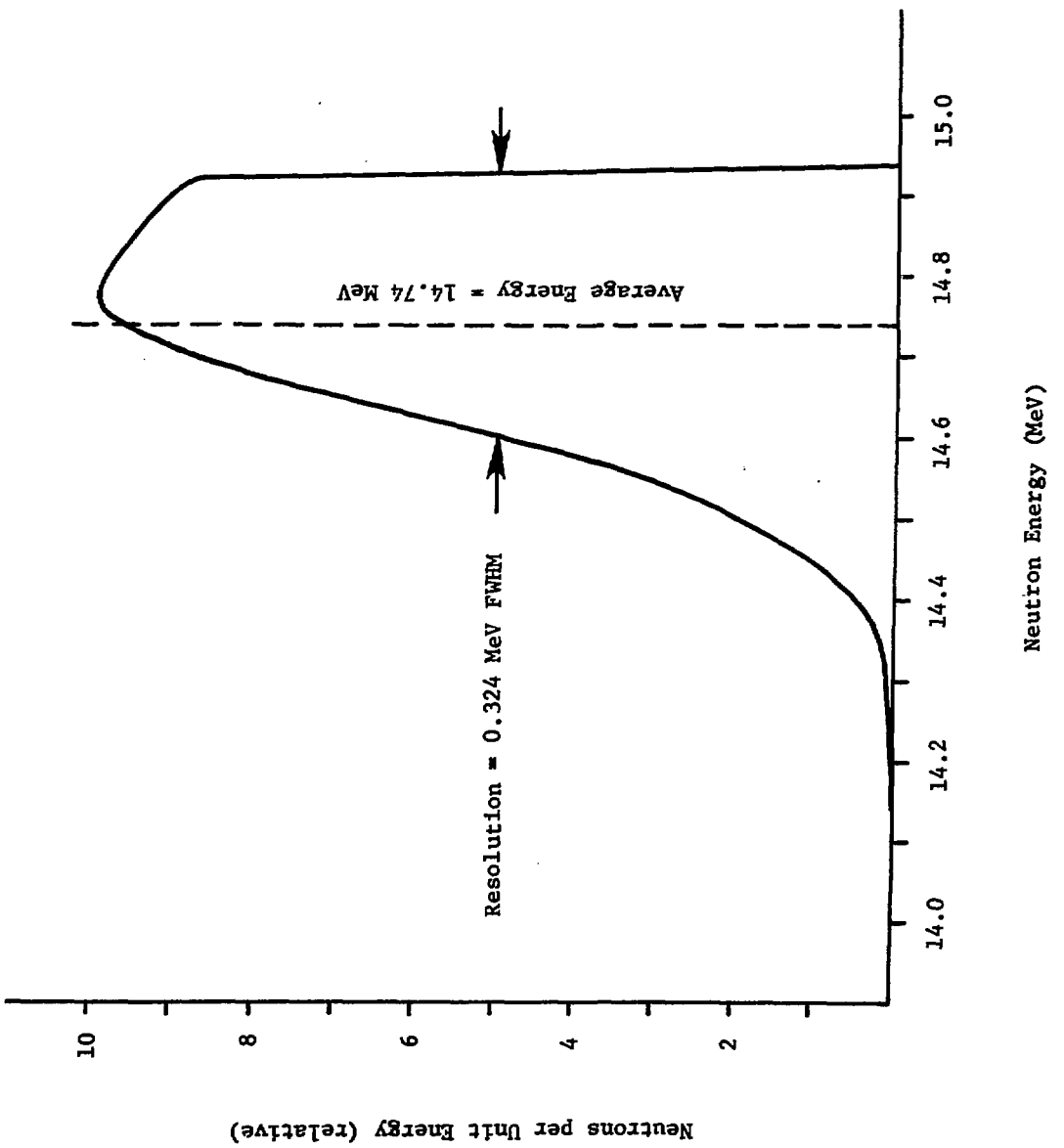
Neutrons per Unit Energy (relative)
2
4
6
8
10
14.0
14.2
14.4
14.6
14.8
15.0
Neutron Energy (MeV)
Average Energy = 14.74 MeV
Resolution = 0.324 MeV FWHM

Figure 6

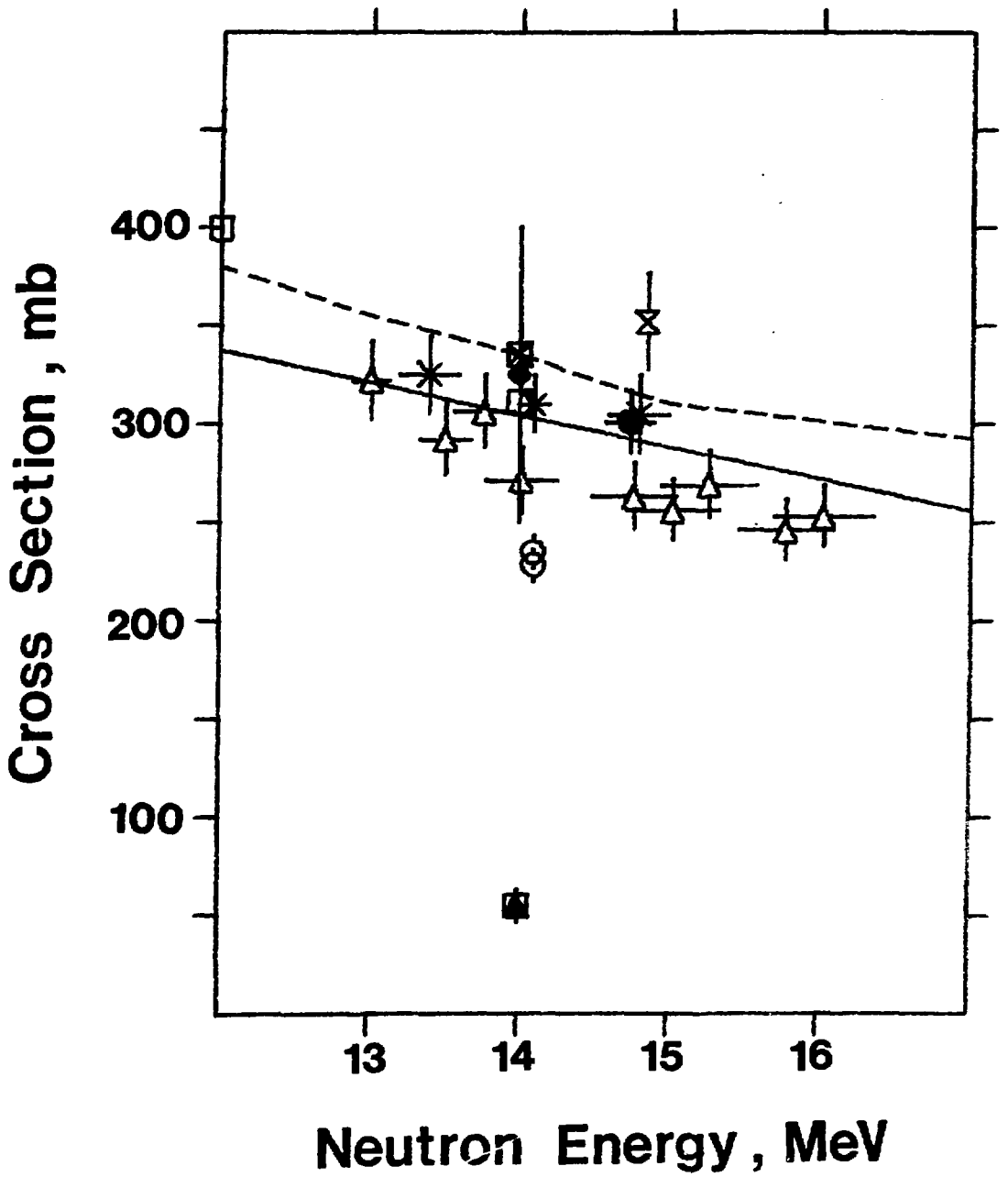
Cross Section, mb
400
300
200
100
13
14
15
16
Neutron Energy, MeV

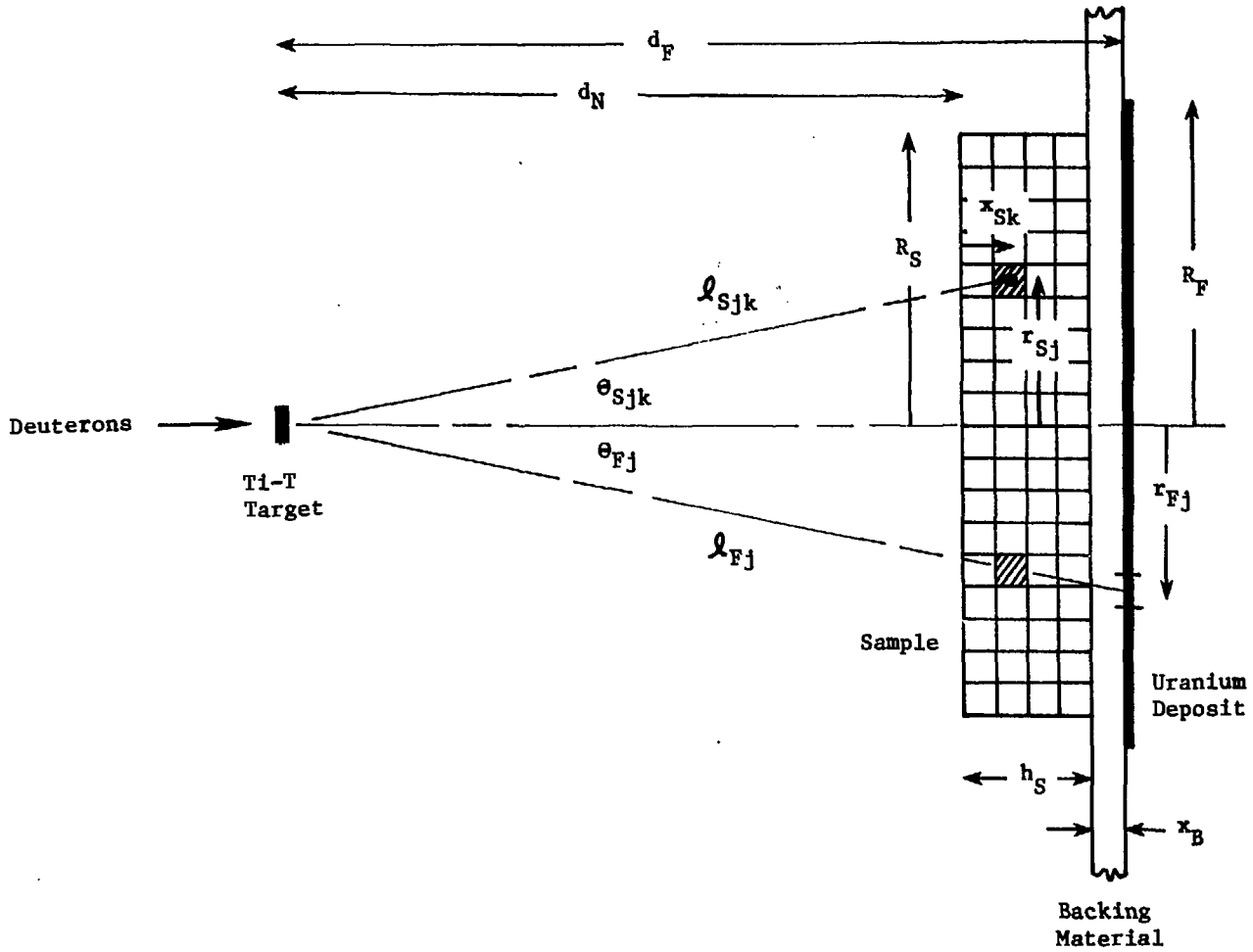
d_F
d_N
R_S
x_{Sk}
ℓ_{Sjk}
r_{Sj}
R_F
θ_{Sjk}
Deuterons
θ_{Fj}
Ti-T
Target
r_{Fj}
ℓ_{Fj}
Sample
Uranium
Deposit
h_S
x_B
Backing
Material

Figure 7